Planetary and Space Science 113-114 (2015) 237–255

Contents lists available at ScienceDirect

Planetary and Space Science

journal homepage: www.elsevier.com/locate/pss

Carbon monoxide short term variability observed on Venus with SOIR/VEX

A.C. Vandaele [a,*], A. Mahieux [a,b], S. Robert [a], R. Drummond [a], V. Wilquet [a], J.L. Bertaux [c]

[a] Planetary Aeronomy, Belgian Institute for Space Aeronomy, 3 av. Circulaire, 1180 Brussels, Belgium
[b] Fonds National de la Recherche Scientifique, 5 rue d'Egmont, 1000 Brussels, Belgium
[c] LATMOS, 11 Bd d'Alembert, 78280 Guyancourt, France

ARTICLE INFO

Available online 18 December 2014

Keywords:
Venus Express
SOIR
CO
Atmosphere composition
Venus

ABSTRACT

The SOIR instrument on board the ESA Venus Express mission has been operational since the insertion of the satellite around Venus in 2006. Since then, it has delivered high quality spectra of the atmosphere of Venus. Spectra are recorded in the IR spectral region (2.2–4.3 μm) using the solar occultation geometry and give access to a vast number of ro-vibrational lines and bands of several key species of the atmosphere of Venus. Here we present the retrieval strategy applied to obtain high quality vertical profiles of carbon monoxide (CO) densities and volume mixing ratios (vmr), spanning the 65–150 km altitude range. We discuss the methodology used to derive the profiles and the validation process implemented to ensure the quality and reproducibility of the results. Influence of ancillary data, such as temperature, is discussed. High variability of CO densities and vmr is observed in relatively short term periods. Correlation between CO and CO_2 densities, as well as between CO and temperature above 110 km, corroborates that the major process at those altitudes is the photodissociation of CO_2 into CO.

1. Introduction

Carbon monoxide (CO) is produced by photodissociation of CO_2 on the day side in the upper atmosphere of Venus by solar UV radiation. Products of the dissociation, CO and O, are transported to the night side by the subsolar-to-antisolar (SS-AS) circulation, most active at high altitudes (above 120 km). The 3-body CO+O recombination reaction into CO_2 is very slow and, alone, cannot explain the low O_2 abundances observed in the Venus atmosphere. Faster recombination processes through catalytic cycles involving chlorine (ClO_x) or hydrogen (HO_x) oxides have been proposed (Krasnopolsky and Parshev, 1983; Krasnopolsky, 2012; Yung and DeMore, 1982) as well as catalytic CO oxidization reactions within the clouds (Mills and Allen, 2007; Mills et al., 2007).

CO abundance above the clouds was first measured by Connes et al. (1968) who deduced a disk-average mixing ratio of 45 ± 10 ppm at 64 km. Krasnopolsky (2008) investigated the latitudinal distribution of CO using the ground-based CSHELL instrument at NASA's Infrared Telescope Facility (IRTF), reporting an average value of 70 ± 10 ppm at 60° latitude and 8 am local solar time for altitudes between 68 and 71 km. Krasnopolsky also indicated a 10% variability of the CO measurement, which he associated to atmospheric dynamics. Observations at millimeter and sub-millimeter wavelengths have shown that the CO abundance is very variable at high altitudes (around 100 km) (Clancy and Muhleman, 1985, 1991; Clancy et al., 2008, 2012b; Gurwell et al., 1995). Irwin et al. (2008) reported latitudinal distribution of CO above the cloud level using VIRTIS-M/VEX observations. They found an average value of 40 ± 10 ppm (at 65–70 km) with little variation in the middle latitudes. CO densities at higher altitudes (100–150 km) were obtained by Gilli (2012); Gilli et al. (2015) using the 4.7 μm non-LTE emission band of CO observed by VIRTIS-H. Iwagami et al. (2010) observed nearly uniform distribution of CO above the clouds consistent with the findings of Krasnopolsky (2008). CO has also been observed below the clouds by ground-based instruments (Bézard et al., 1990; Crovisier et al., 2006; Lellouch et al., 1994; Marcq et al., 2014, 2005, 2006; Pollack et al., 1993) and VIRTIS on board Venus (Marcq et al., 2014, 2006; Sung and Varanasi, 2005).

The Solar Occultation in the IR (SOIR) instrument has been designed to measure spectra of the Venus atmosphere in the IR region (2.2–4.3 μm) using the solar occultation technique (Nevejans et al., 2006). This method derives unique information on the vertical composition and structure of the mesosphere and lower thermosphere (Fedorova et al., 2008; Mahieux et al., 2010, 2012; Vandaele et al., 2008). SOIR is an extension mounted on top of the SPICAV instrument (Bertaux et al., 2007a). SPICAV/SOIR is one of the seven instruments on board Venus Express, a planetary

* Corresponding author.
E-mail address: a-c.vandaele@aeronomie.be (A.C. Vandaele).

http://dx.doi.org/10.1016/j.pss.2014.12.012
0032-0633/

mission of the European Space Agency (ESA) that was launched in November 2005 and inserted into orbit around Venus in April 2006 (Titov et al., 2006). The SOIR instrument is unique in terms of spectral coverage and spectral resolution (0.15 cm^{-1}), and is ideally designed to probe the Venus atmosphere, above the cloud deck, for CO_2 as well as trace gases. CO is particularly well covered since the (2-0) band strongly absorbs in the 3900–4400 cm^{-1} range, which is well inside the sensitivity range of the SOIR instrument.

The instrument will be described briefly in the following section. The CO spectroscopy is presented next, followed by a detailed description of the method used to derive the vertical profiles of CO densities directly from the SOIR spectra. Since CO_2, the major component of the atmosphere, is also measured with the same instrument, sometimes even simultaneously during the same occultation, CO volume mixing ratios (vmr) can be obtained. We will also present the method developed to derive CO vmr when no concomitant CO_2 is measured. Detailed analysis of several selected periods of observation will then be performed. These observations were selected in order to derive information on the short term variability of CO.

2. Instrument description

The instrument has already been extensively described elsewhere (Bertaux et al., 2007b; Mahieux et al., 2008; Nevejans et al., 2006) and will only be briefly outlined here. SOIR is an Echelle grating spectrometer operating in the IR, combined with an acousto-optic tunable filter (AOTF) for the selection of the recorded wavenumber interval. The wavenumber range covered by the instrument extends from 2200 to 4370 cm^{-1} (2.2–4.3 μm) and is divided into 94 diffraction orders (from 101 to 194). The definition and limits of these diffraction orders are presented in Vandaele et al. (2013). The bandwidth of the AOTF was originally designed to be 20 cm^{-1}, as measured on ground before launch (Nevejans et al., 2006), to allow light from only one order into the spectrometer. However, the measured bandwidth of the AOTF filter is ~24 cm^{-1} (Mahieux et al., 2008), creating some order leakage on the detector, since it is wider than one diffraction order. Information from adjacent orders leaks onto the detector. This effect is called superposition of orders hereafter.

The detector is made up of 320 pixels along the spectral axis and 256 rows. The instrument entrance slit is projected on 32 rows. Due to telemetry limitations, only the equivalent of 8 rows per second can be downlinked to Earth. In most of the observations 4 different values of the AOTF frequency are chosen to record spectra in 4 different spectral intervals per second, hence increasing the number of species potentially detectable simultaneously. In that case, only 2 spectra per AOTF frequency can be downlinked, corresponding to 2 'bins' of rows on the detector. It was noticed early on that the outermost rows of the slit projection on the detector were not fully illuminated, so only the 24 central rows were considered after orbit 332 (March 19, 2007), leading to the definition of 2 bins of 12 rows each (compared to the 2 bins of 16 rows that were considered before orbit 332).

The resolution of the SOIR instrument varies slightly from the first to the last order, from 0.12 to 0.20 cm^{-1}, as does the spectral sampling interval which varies from 0.030 cm^{-1} in diffraction order 101–0.055 cm^{-1} in order 194, increasing with the pixel number and the diffraction order. Signal to noise ratio on the SOIR transmittances varies between 250 and 5000 but is typically of the order of 2000. These SNR values are deduced from the recorded spectra as explained in Vandaele et al. (2013). The spectra used in this work are PSA Level 3 calibrated data, which have been intensively described in Vandaele et al. (2013).

3. CO spectroscopy

The CO molecule presents two absorption bands in the spectral interval covered by the SOIR instrument. The most intense one (1-0) is active in the 2000–2250 cm^{-1} region, which lies at the limit of the SOIR sensitive range. However, intense CO_2 absorption overlaps the CO signature in that region, and those CO features cannot be used. The (2-0) band covers the 3900–4400 cm^{-1} spectral interval, as can be seen in Fig. 1, where the positions and line intensities are from HITRAN 2008 (Rothman et al., 2009).

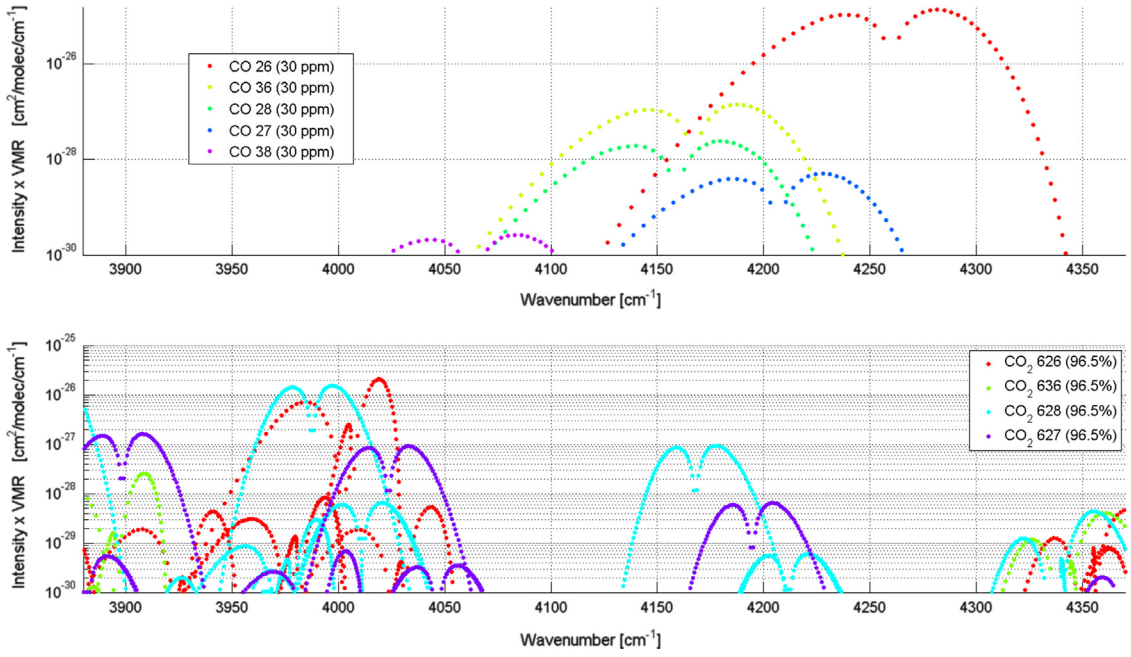

Fig. 1. CO and CO_2 absorption features in the 3900–4400 cm^{-1} spectral interval. Line intensities from HITRAN 2008 (Rothman et al., 2009) have been multiplied by typical vmr values (96.5% for CO_2, 30 ppm for CO). Only lines with a final intensity higher than 1.0×10^{-30} cm^2/molecule/cm^{-1} are considered.

In fact, another band, the (3-1) is also located in that spectral range, but with smaller intensities. All isotopologues of CO are shown, the notation being the one defined in HITRAN (the main isotopologue $^{12}C^{16}O$ being designated by CO 26). Isotopic ratios were considered to be the same on Venus as on Earth (Bézard et al., 1987; Clancy and Muhleman, 1991). Typical intensities of observed lines are presented in Fig. 1 for both CO and CO_2, where line intensities from HITRAN have been multiplied by typical values of volume mixing ratio: 96.5% for CO_2 and 30 ppm for CO. This figure, which was obtained for an altitude of 100 km (temperature = 171 K and pressure = 2.4×10^{-2} mbar) shows that the CO (2-0) band is the main absorber in this region and its detection should not be impacted by the presence of CO_2 absorption structures. In particular, CO density profiles have been retrieved from spectra recorded in orders 185–194 (4130–4380 cm^{-1}). The altitude range probed depends on the strength of the absorption lines considered. By combining different orders, i.e. different line intensities, CO profiles can be provided from 65 up to 150 km altitude.

Broadening coefficients have been modified from the HITRAN reported Earth-like air conditions to take into account the presence of CO_2 as the main buffer gas. Sung and Varanasi (2005) reported CO_2-broadened half-widths and CO_2-induced line shifts for the fundamental (1-0) of $^{12}C^{16}O$ at 201, 244, and 300 K, as well as for the first (2-0) overtone and the second (3-1) overtone bands at 298 K. We have considered their values for the lines in common with the HITRAN database, corrected for the temperature, HITRAN's reference temperature being 298 K. The lines which are not reported in Sung and Varanasi have been corrected by a conversion factor air-width to CO_2-width derived from the comparison of available common values. The temperature coefficient has been held constant for all lines ($n = 0.73$), as suggested in Sung and Varanasi (2005). The correction applied to the broadening coefficients is illustrated in Fig. 2. Laboratory observations (Sung and Varanasi, 2005), uncorrected air broadening coefficients from HITRAN, as well as HITRAN values corrected for the presence of CO_2 are all plotted together and compared. The correction has been applied by considering all lines from the (1-0) and (2-0) bands common to HITRAN and Sung and Varanasi (2005), weighted by the measurement uncertainty. Whilst willing to use the best available and more correct values of the broadening coefficients, the SOIR resolution (0.15–0.2 cm^{-1}) precludes any sensitivity to the pressure broadening of the lines (Vandaele et al., 2013). As an example, the FWMH value at infinite resolution of the R7 line of the (2-0) band of CO at 4288.29 cm^{-1}, corresponding to a temperature of 200 K and a pressure of 10 mbar is 0.00935 cm^{-1}, almost 20 times narrower than the SOIR resolution in that order (0.2 cm^{-1}). The broadening effect becomes more pronounced with increasing pressure however.

4. CO densities and mixing ratios retrieval

4.1. Description of the method

4.1.1. Simulation of SOIR spectra

The retrieval method has been fully described in Mahieux et al. (2010, 2012) in the case of CO_2 density retrievals. It will be summarized here and adapted when necessary to the detection of trace gases, such as CO.

The solar occultation technique used by SOIR allows the derivation of unique information about the vertical structure and composition of the Venus mesosphere (Vandaele et al., 2008). SOIR is looking towards the Sun and records spectra on a one second cycle basis. Solar occultations occur when the line of sight (LOS) of the instrument crosses the atmosphere of Venus. The projection of the center of the slit on the limb during each single measurement defines the tangent altitude. Because the spacecraft is moving along its orbit, the instrument sounds the atmosphere of the planet at different tangent altitudes. The attitude of VEX is calculated using the Spice routines developed by NAIF (NASA Ancillary Information Facility, Acton (1996)), and used by ESA for the Venus Express mission.

The transmittance $T_{L,Molecular}$ due to all molecular species present along the LOS path corresponding to the tangent height L is obtained by multiplying the absorbance of all molecules in all

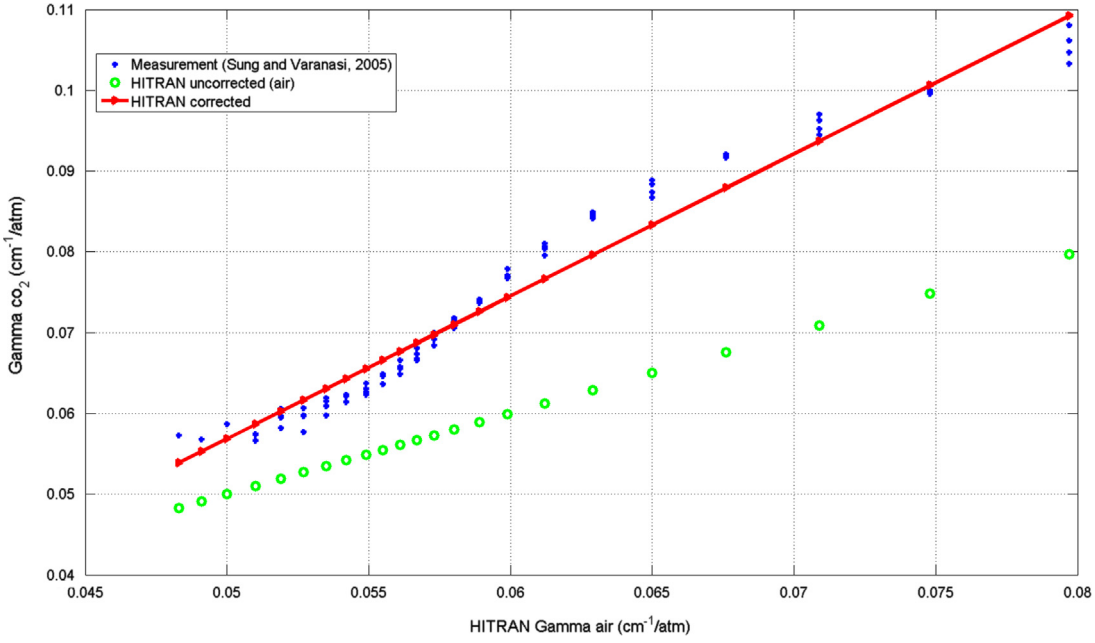

Fig. 2. Correction applied on the HITRAN data to obtain CO broadening coefficients under a CO_2-rich atmosphere. Blue stars are the measurements performed by Sung and Varanasi (2005), green circles are the HITRAN uncorrected values (air broadening) and the red triangles are the corrected HITRAN values. The correction has been applied by considering all lines common to HITRAN and Sung and Varanasi (2005), weighted by their measurements uncertainty.

the layers crossed

$$T_{L,Molecular} = \prod_{j=1}^{L} \prod_{i=1}^{n_{molecules}} T_{i,j} \quad (1)$$

where the transmittance $T_{i,j}$ due to molecule i in layer j is calculated using

$$T_{i,j} = \exp\left[-n_{i,j} s_j ACS\left(t_j, p_j\right)\right] \quad (2)$$

where $n_{i,j}$ is the density of the molecule i in layer j, s_j is the path length within layer j, and t_j and p_j are the temperature and the pressure in layer j. The molecular absorption cross sections (ACS) in each layer are calculated by a line by line procedure, extensively described in IASB-BIRA (2013); Vandaele et al. (2008). They depend on the partial and total pressures, as well as on the temperature in each layer.

The baseline of each transmittance is simulated as a polynomial. In general a polynomial of order 2 is enough to reproduce the shape of the observed baseline

$$T_{L,Baseline} = a_L + (\omega_n - \omega_{n_0}) b_L + (\omega_n - \omega_{n_0})^2 c_L \quad (3)$$

where a_L, b_L and c_L are the polynomial coefficients, ω_n is the wavenumber, ω_{n_0} is the central wavenumber of the scanned order. This baseline is linked to the extinction due to the aerosols present along the line of sight. The treatment of the baseline in terms of aerosol content has been described in detail by Wilquet et al. (2012, 2009).

The synthetic spectrum I_L, which will be compared to the one recorded by the instrument, is the solar spectrum attenuated by the effect of the atmospheric molecular species and aerosols, convolved by the instrumental function

$$I_L = \left(\underbrace{I_{Sun} \cdot T_{L,Baseline} \cdot T_{L,Molecular}}_{\text{synthetic spectrum}}\right) \otimes \left(\underbrace{ILS(Resol_{SOIR})}_{\text{instrument function}}\right) \quad (4)$$

with I_{Sun} the Sun radiance (Hase et al., 2010) and $ILS(Resol_{SOIR})$ the instrument function with the spectral resolution function of SOIR (Vandaele et al., 2013).

As previously explained in the instrument description, the bandwidth of SOIR's AOTF, used for the diffraction order selection, is larger than the free spectral range of the echelle grating. To correctly simulate the spectra measured by the spectrometer, the contribution of adjacent orders also has to be taken into account. Usually, the three first adjacent orders and the central order are considered to form most of the observed transmittance. Finally transmittances are calculated by dividing the simulated spectrum by the equivalent full Sun spectrum (convolved by the instrumental function, $I^{\otimes}_{Sun}$)

$$T = \frac{\sum_{i=-n_{orders}}^{n_{orders}} AOTF_i I_L}{\sum_{i=-n_{orders}}^{n_{orders}} AOTF_i I^{\otimes}_{Sun}} \quad (5)$$

where T is the final transmittance, n_{orders} is the number of adjacent orders considered on each side of the central order, $AOTF_i$ is the values of the AOTF transfer function in the order i.

To account for the physical size of the slit and the corresponding effect on the vertical resolution of the instrument, an improvement has been implemented into the retrieval algorithm (Mahieux et al., 2015). In the previous version, the ray tracing was calculated by considering only one light path corresponding to line of sight (LOS) defined between the tangent height and the center of the selected bin on the slit. Since the vertical resolution of the instrument varies a lot with the latitude of the measurement, this introduced a bias in the retrieval. This would be seen in the results as an altitude shift with latitude. In the improved algorithm, 24 light paths spread across the slit in both directions are now considered, and the measurement at one altitude level is calculated as the algebraic average of the contributions of all paths.

4.1.2. The retrieval method

The retrieval algorithm is based on the Optimal Estimation (OE) method developed by Rodgers (1990, 2000), considering all spectra of one single solar occultation together. The different tangent heights define the layering of the atmosphere, in which the densities $n_{i,j}$ are retrieved. Details of the implementation of the method can be found in Mahieux et al. (2010). Different isotopologues of one species can be retrieved separately, however in this study, the retrieval of the CO density made no distinction between the different isotopologues observed. We have indeed considered that the isotopic ratios on Venus were the same as on Earth for C and O atoms (Bézard et al., 1987; Clancy and Muhleman, 1991).

One crucial parameter in the Rodgers OE method is the *a priori* knowledge that we have of the variables to retrieve. This covers the *a priori* profile and the covariance matrix which represents the variability of the variable considered. These two quantities should be the best knowledge we have of the problem to solve before starting the analysis of the spectra: the *a priori* profile is taken from the VIRA model (Hedin et al., 1983; Seiff et al., 1985) for trace gases and from the VAST (Venus Atmosphere from SOIR measurements at the Terminator) model for the CO_2 density. In this study we have considered diagonal elements of the covariance matrix S_a to represent a possible variation of 25% around the *a priori* density (in logarithm) and non-diagonal elements given by

$$S_a(i,j) = \sqrt{S_a(i,i) S_a(j,j)} \exp\left(-\left(\frac{z_i - z_j}{l_c}\right)^2\right) \quad (6)$$

to account for correlation between the densities at different altitudes. The choice of the 25% variability was the result of a thorough sensitivity study that was performed on different parameters appearing in the retrieval method (Mahieux, 2011). In Eq. (6), z_i and z_j are the heights between which the correlation is calculated and l_c is the correlation length, which corresponds to 2 scale heights.

The retrieval is thus applied on all spectra acquired during one occultation, i.e. on spectra recorded in each bin of the detector and in all 4 spectral intervals, selected by the 4 possible settings of the AOTF (8 spectra per second). By retrieving information simultaneously in all 4 spectral ranges, the method ensures the coherence of the results. Indeed suppose that one order gives access to CO_2 (and indirectly to temperature, see Mahieux et al. (2012)), these CO_2 density and temperature values will be used to define the total density and volume mixing ratio of the different trace gases that might be detected using the other spectral ranges recorded at the same time. This method also guarantees the coherence of the results for one given species, when several intervals contain information on this particular species.

The method is illustrated with the analysis of the spectra recorded during orbit 706 (27/03/2008). The 4 different orders recorded during this specific orbit are orders 149, 166, 190, and 191, corresponding to the 3329–3359 cm^{-1}, 3709–3742 cm^{-1}, 4246–4283 cm^{-1}, and 4268–4305 cm^{-1} spectral intervals respectively. CO absorption features are present in the 190 and 191 intervals, while CO_2 lines are present in orders 149 and 166. Fig. 3 illustrates the quality of the fit of some individual spectra. In this example, spectra obtained in the 4280–4300 cm^{-1} region (order 191) are shown for six altitudes out of 40 available for this occultation. For each altitude the observed SOIR spectrum (in blue) and the fitted one (in green) are presented along with the differences between them. Fig. 4 illustrates the method and convergence and Fig. 5 presents the final results. All individual CO and CO_2 densities retrieved from different spectra belonging to one of the 4 spectral ranges (all bins considered) are shown as dots

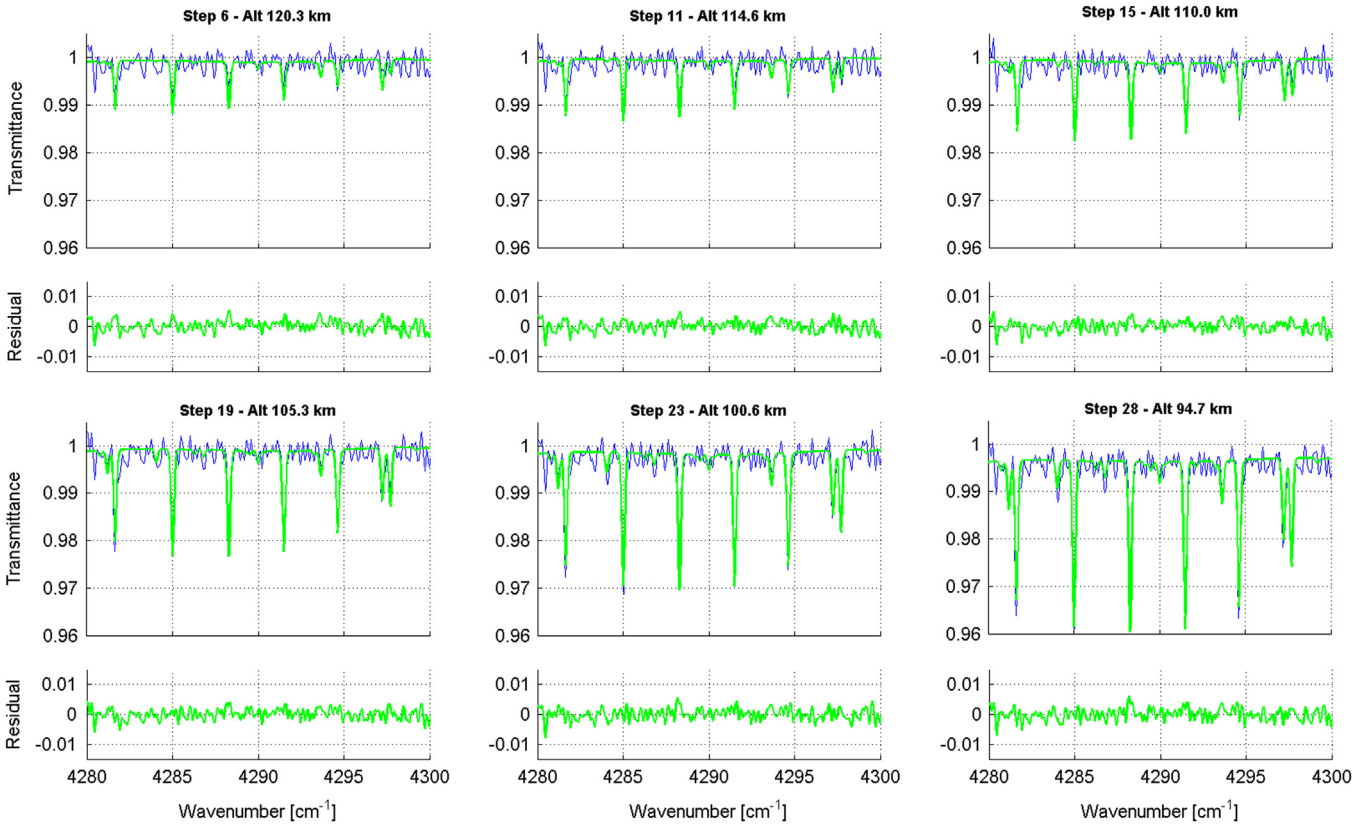

Fig. 3. Examples of spectra analysis corresponding to the order 191 at the final step of the procedure (orbit 706, bin 1). Six altitudes are shown here. The altitudes are indicated on top of each sub-plot. The observed spectrum (blue) and the fitted one (green) are shown for each of the altitudes, along with the differences between the observed and fitted spectra.

in the figures. The different colors in Fig. 4 indicate the iteration number: at the first iteration, all 4 spectral intervals are analysed in parallel and independently; then the individual density values leading to the detection of CO_2 (from orders 149 and 166) are combined to provide one single profile of CO_2. Similarly a single CO profile is obtained by considering all points from orders 190 and 191. The density vertical profiles (plain lines in Fig. 4) are obtained by applying a weighted linear moving average: at a given altitude the final density will be the average value of all individual values lying within two scale heights, weighted by their individual errors. These density profiles will then be the starting point for the next iteration. In this way, the new '*a priori*' density profile takes into account information from all available spectral intervals, and covers an extended altitude range. Moreover, temperature, derived from the CO_2 density by applying the hydrostatic relation, will also change from one iteration to the next. In that case, since temperature is deduced at each step from the CO_2 density (Mahieux et al., 2012), the method ensures that temperature is also 'fitted' in this iterative way and is used for the determination of all possible targeted species. Convergence is achieved when two successive density profiles agree within their respective error bars at all altitudessq and for all species included in the retrieval. In this particular case, convergence was achieved after 3 iterations. However it should be noted that doing this, the method we have developed is not exactly the one proposed by Rodgers (2000), since the new '*a priori*' knowledge also contains information from the data themselves. Rodgers (2000) has shown that using the results from the previous iteration as '*a priori*' reduces the speed of convergence.

At the start of the procedure, all spectra satisfying the criteria on the altitude range selection are considered. These criteria, defined in Mahieux et al. (2012) concern the determination of the first and last spectra corresponding respectively to (1) the highest altitude when the absorption due to the targeted species starts to rise above the noise level and (2) the lower altitude when the observed absorption lines of the targeted species are saturated. As the fitting procedure evolves, these limits are adapted. This can be seen in Fig. 4 (iteration 2 on CO, Panel A), where the retrieved CO density values implied that the lines in the observed spectra were saturated below 85 km. Finally one supplementary test is applied to keep or not the values of the retrieved local density based on the use of the Degree Of Freedom (DOF) returned by the OE procedure. The DOF represents the number of independent values (*ndof*) that can be retrieved from the data set. Only the first *ndof* highest eigen values of the OE retrieval will be kept. This reduces in general the number of actual values but ensures that only values which contain real information coming from the observations are considered. In general, the values that are rejected correspond to the highest altitudes where the signature of the targeted species is too close to the noise level.

The final results are illustrated for CO in Fig. 5. When considering each spectral interval separately, four density profiles are obtained, shown in blue (order 190, bin 1), cyan (order 191, bin 1), orange (order 190, bin 2) and red (order 191, bin 2). They start and end at different altitudes depending on the strength of the lines present in each of the orders: intense lines provide information on the highest layers where CO concentration is lower, whereas weaker lines deliver information on the lowest layers. The final CO density profile is again the results of a running average of all individual density values, weighted by their uncertainties. For this last step, it is possible to perform the running

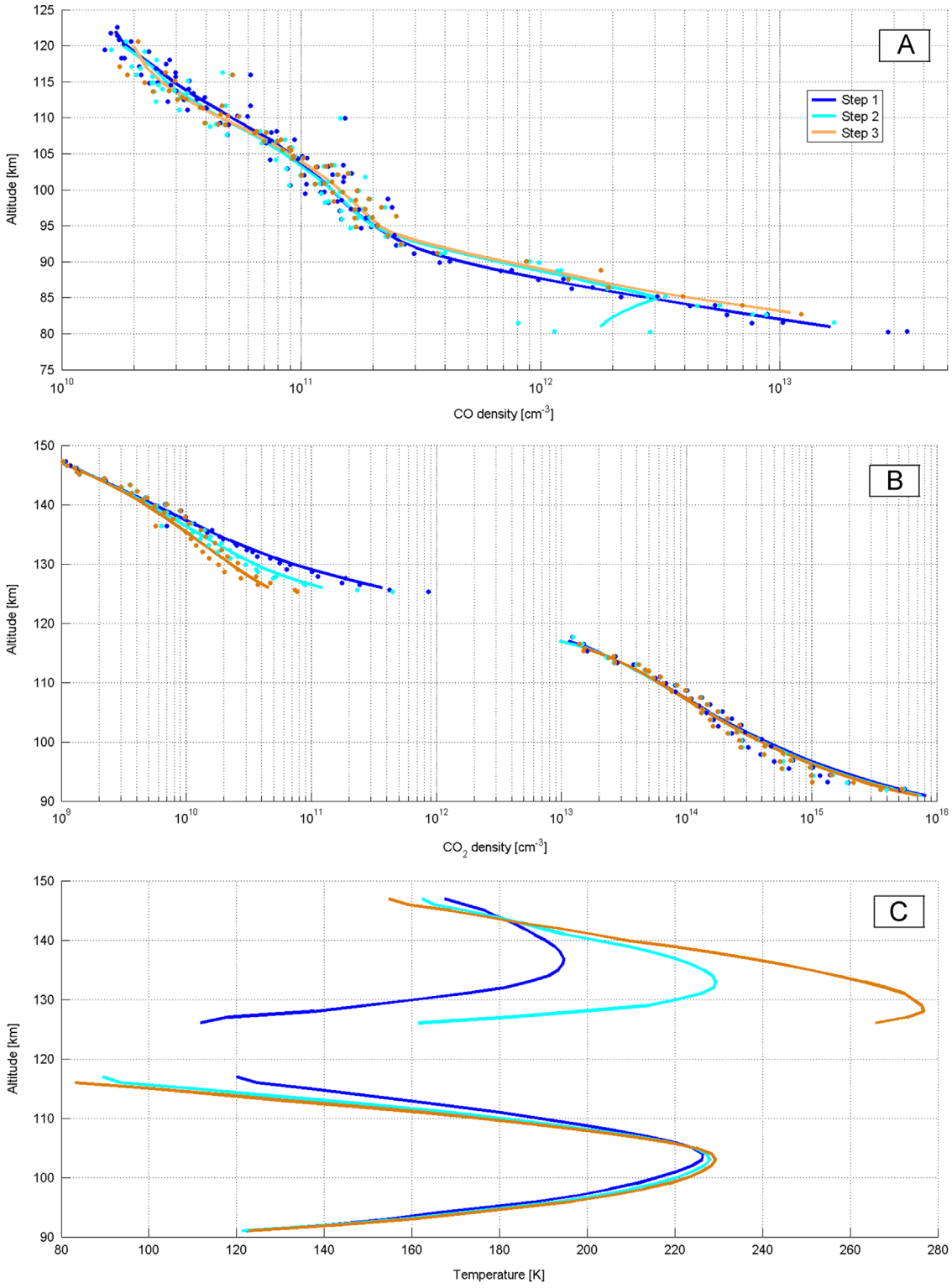

Fig. 4. Convergence of the retrieval method for CO (A), CO_2 (B) and temperature (C) illustrated for Orbit 706. At step 1 (dark blue), the 4 spectral ranges (all bins considered) are analysed separately. Individual local density values are represented by the dots. Then, a single density profile (dark blue line) is built by a running average on all individuals dots over two scale heights. This is used as the '*a priori*' density profile for the next iteration. Convergence was achieved after 3 iterations in this example, the orange lines are the final CO and CO_2 density profiles and associated temperature.

average by considering multiples or fractions of the scale height. In this particular example, the final profile has been obtained with an averaging over one scale height.

The primary results deduced from the analysis of SOIR spectra are thus densities. Conversion to volume mixing ratio (vmr) requires the knowledge of the total density, or that of CO_2, if a CO_2 vmr is assumed

$$vmr_{CO} = \frac{n_{CO} \times vmr_{CO_2}}{n_{CO_2}} \tag{7}$$

Two cases are encountered: either the CO_2 density is retrieved simultaneously from one of the 4 orders dedicated to its detection

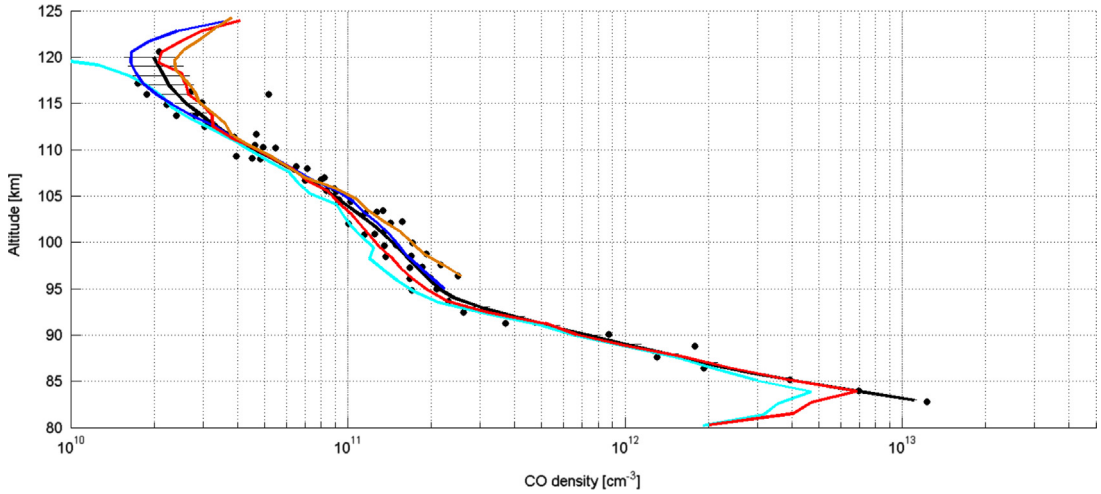

Fig. 5. Illustration of the retrieval method applied on orbit 706. The dots represent the individuals CO density retrieved at different altitudes from one spectrum recorded during orbit 706 (bins 1 and 2 of orders 190 and 191). When considering each spectral interval separately, four density profiles are obtained, shown in blue (order 190, bin 1), cyan (order 191, bin 1), orange (order 190, bin 2) and red (order 191, bin 2). The final CO density vertical profile (black line) is obtained directly from all the individual dots, by applying a moving average: at a given altitude the final CO density will be the average value of all individual values lying within one scale height, weighted by their individual errors.

and is directly used to obtain the CO vmr using Eq. (6), or no information on CO_2 is available from the observation itself. In that case, the CO_2 density will be derived from the VAST model, which has been described in detail in Mahieux et al. (2012) and updated in Mahieux et al. (2015). In both cases, an assumption is made on the CO_2 mixing ratio (vmr_{CO2}), whose values are taken from the VIRA model – data from Seiff et al. (1985) for altitudes up to 100 km and from Hedin et al. (1983) above that altitude – have been used. In the following, CO vmr will be shown only at altitudes where CO_2 densites retrieved from the same occultation were available.

4.2. Sensitivity study

From the description of the method and of the instrument, it appears that several parameters may have an influence on the retrieved densities of CO. The full description of the sensitivity study performed on SOIR retrievals in the case of CO_2 can be found in Mahieux (2011). In the present work we have adapted this study to the retrieval of CO retaining only two major parameters, i.e. the temperature and the number of orders included in the order superposition. In the following the influence of both parameters will be examined in detail.

Considering first the impact of the choice of the temperature profile on the retrieval of the CO density, different temperature profiles were used for the sensitivity study: 2 isothermal profiles corresponding to 150 K and 200 K; the VIRA model (data from Seiff et al. (1985) for altitudes up to 100 km and from Hedin et al. (1983) above that altitude), and the VAST model (Mahieux et al., 2012). Moreover, profiles ± 20 K relative to VAST and VIRA were also considered. In total 8 temperature profiles were used, shown in Fig. 6. The complete test was performed for one orbit where all four orders were dedicated to CO. Results of the sensitivity analysis are shown in Fig. 7 for the order 191, similar results were obtained for the other orders used to derive CO. First, both VIRA and VAST, although different in shape, produce very similar CO densities at all altitudes, including those corresponding to the warm layer situated at 105 km and the cold layer above that present in the VAST temperature profile. The same can be said for the VAST ± 20 K and VIRA ± 20 K profiles. The differences start to appear below 95 km. The error on the CO density (Fig. 7, Panel B) remains of the same order of magnitude for the 6 profiles built on VAST and VIRA. The root mean square (rms) of the (fitted – observed) transmittance does not change either (Fig. 7, Panel C). The largest discrepancies (in density, but also in error and rms) are obtained when using the two isothermal profiles. Errors for the isothermal profiles start to increase at lower altitudes. This is the consequence of the build-up of the discrepancies between simulated and observed absorption features as absorption accumulates in the lower layers. These results are encouraging, indicating that the determination of the CO density is not influenced by the *a priori* temperature profiles, provided that the profile is realistic.

The second parameter which has been investigated is the number of adjacent orders taken into account when simulating the order superposition effect (Eq. (5)). Several cases are considered: only the central order is simulated without any adjacent order ($n=0$), then increasing the number from 1 to 4 on each side of the central order. Note that the default value used in almost all retrievals corresponds to $n=3$. Results of the sensitivity study are shown in Fig. 8 for order 189, similar results were obtained for the other orders. Clearly, only considering the central order is not sufficient to reproduce the observed spectra. However convergence is achieved very fast when the first two adjacent orders ($n=1$) are at least included. No gain is added by considering $n=4$ compared to $n=3$, which confirms that this value is a good compromise between computation speed (the larger the number, the more time consuming is the simulation) and accuracy, not only for CO_2, but also for trace gases.

5. Short term variability of CO

In this paper, we want to address the short term variability of CO in the Venus mesosphere and thermosphere. We have selected four particular sets of observations. Each selected set corresponds to a series of occultations which were performed on a short time period. Fig. 9 shows all observations performed by SOIR during the first 14 Occultation Seasons (OS). The boxes indicate the 4 periods selected for this study. For each of these groups of observations, several occultations were carried out regularly over a short period of time. These were also selected on the criteria that latitude should not vary too much, in order to differentiate between vertical resolution effect, latitudinal variation and short time variation. Three groups of occultations have been obtained at

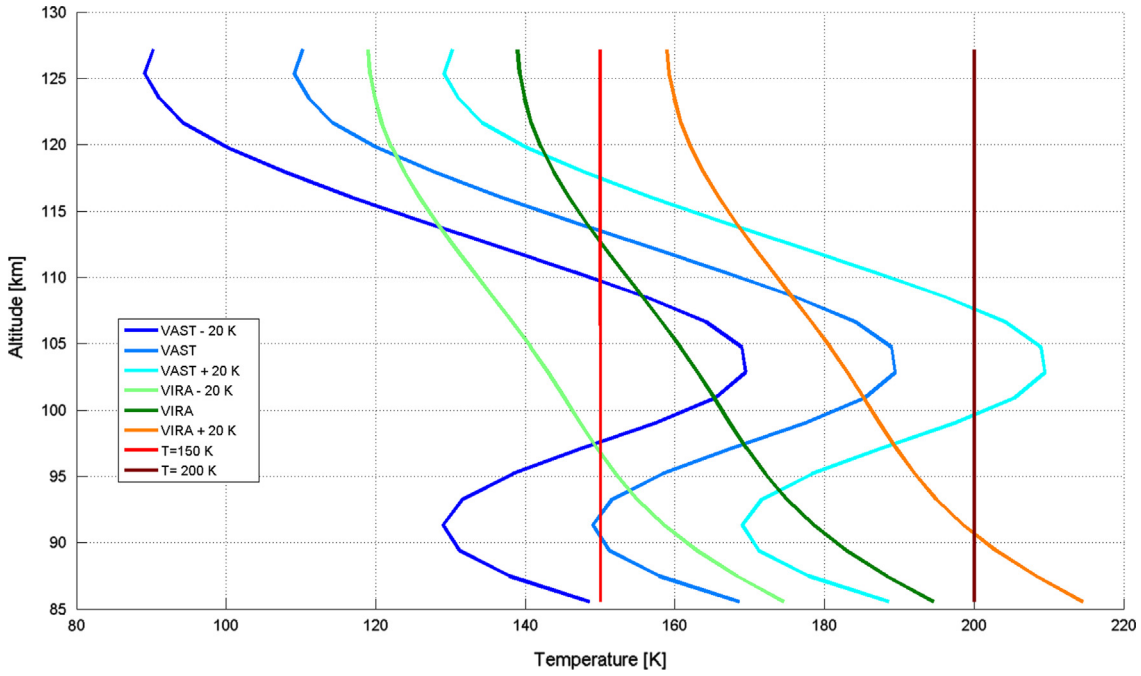

Fig. 6. Different temperature profiles used for the sensitivity study: two isothermal profiles corresponding to 150 K and 200 K, the VIRA model (Hedin et al., 1983; Seiff et al., 1985) and VIRA ± 20 K, and the VAST model (Mahieux et al., 2012), with VAST ± 20 K.

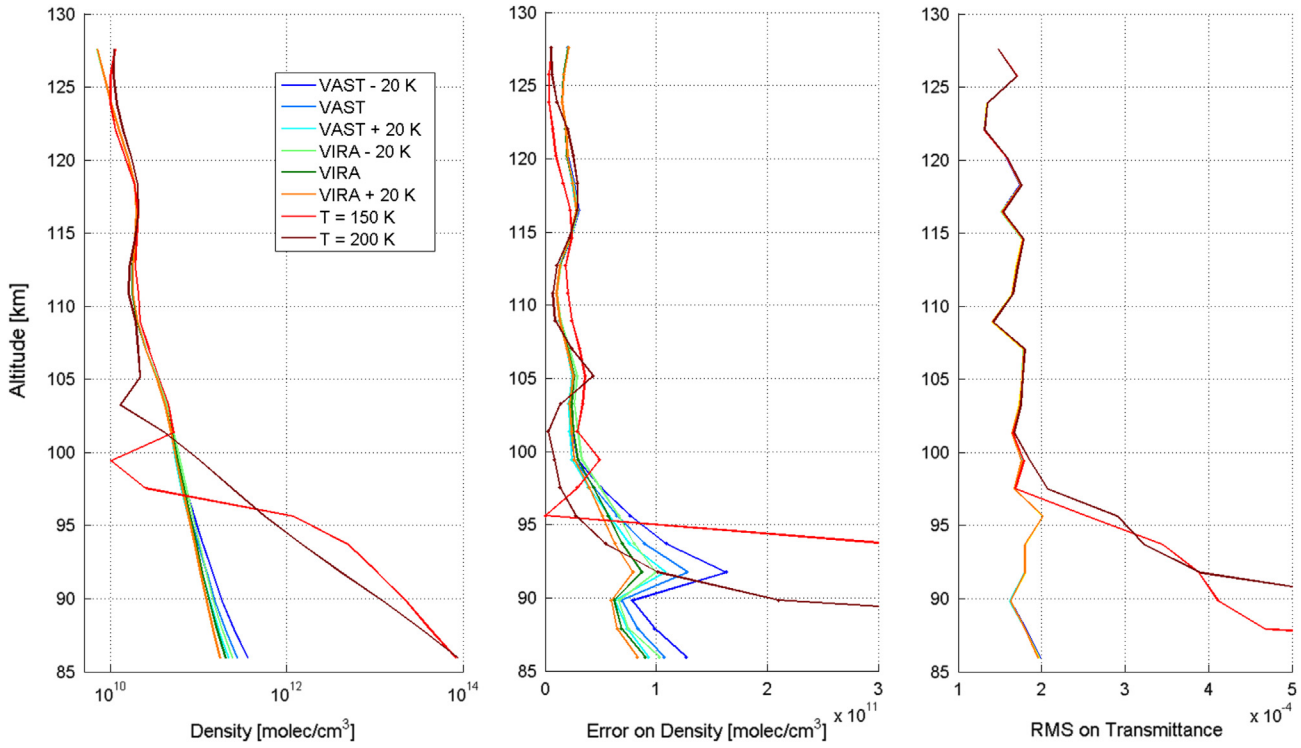

Fig. 7. Results of the sensitivity study on the influence of the temperature on the CO density retrieval (orbit 118, order 191, bin 1). The retrieved densities are shown on the left for each temperature profile, and the associated error on the derived densities in the middle panel, with the root mean square values of the fitted-observed transmittance on the right.

latitudes between 60° and 90°N, and one at latitude 45–90°S. Moreover, at such high latitudes, solar local time has no real meaning, and can be thus considered not to influence the interpretation of the results (valid for OS 8 and 12 in the following). Details on the selected orbits are presented in Table 1,where orbit number, date, solar local time, and latitude are given for each observation. Orders recorded during each occultation are also given with an indication of which species were targeted. In all the selected observations, CO and CO_2 densities were obtained simultaneously, so that CO vmr are defined using Eq. (6) in which the local CO_2 concomitant densities are considered along with CO_2 vmr from the VIRA model.

Results of the analysis of these four selected time periods are shown in Figs. 10–13, where CO densities and vmr are plotted for all orbits, as well as concomitant CO_2 densities. Temperatures obtained for the orbits of OS 8 are also shown. CO decays rapidly

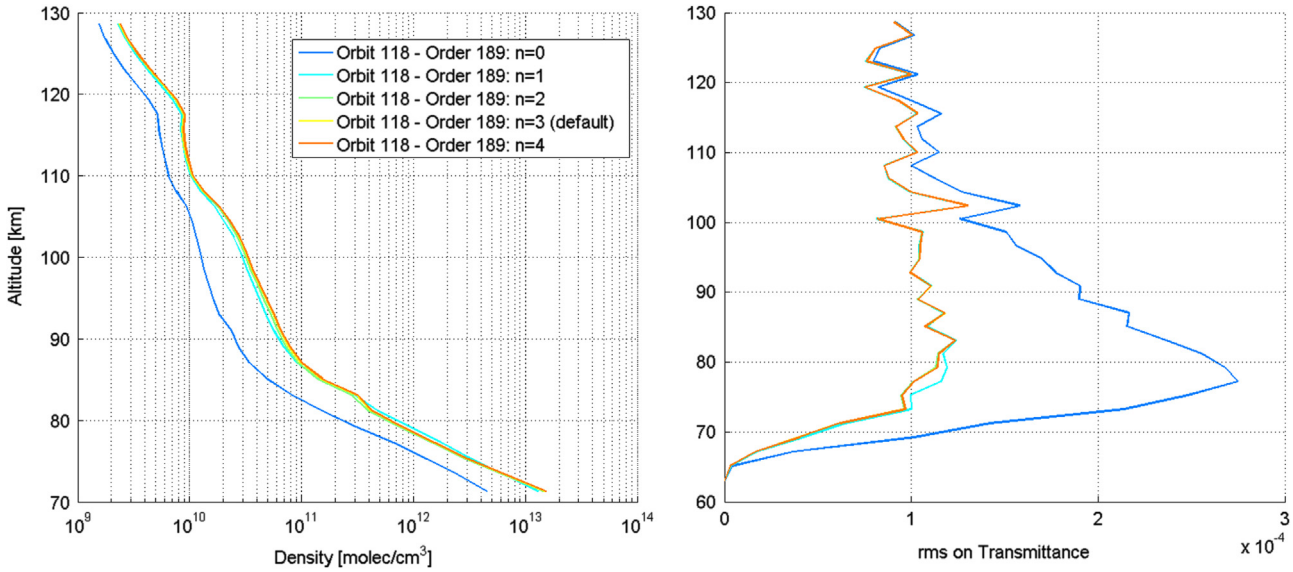

Fig. 8. Sensitivity study of the number of adjacent orders taken into account to simulate a SOIR spectrum (applied on orbit 118, order 189, bin 1).

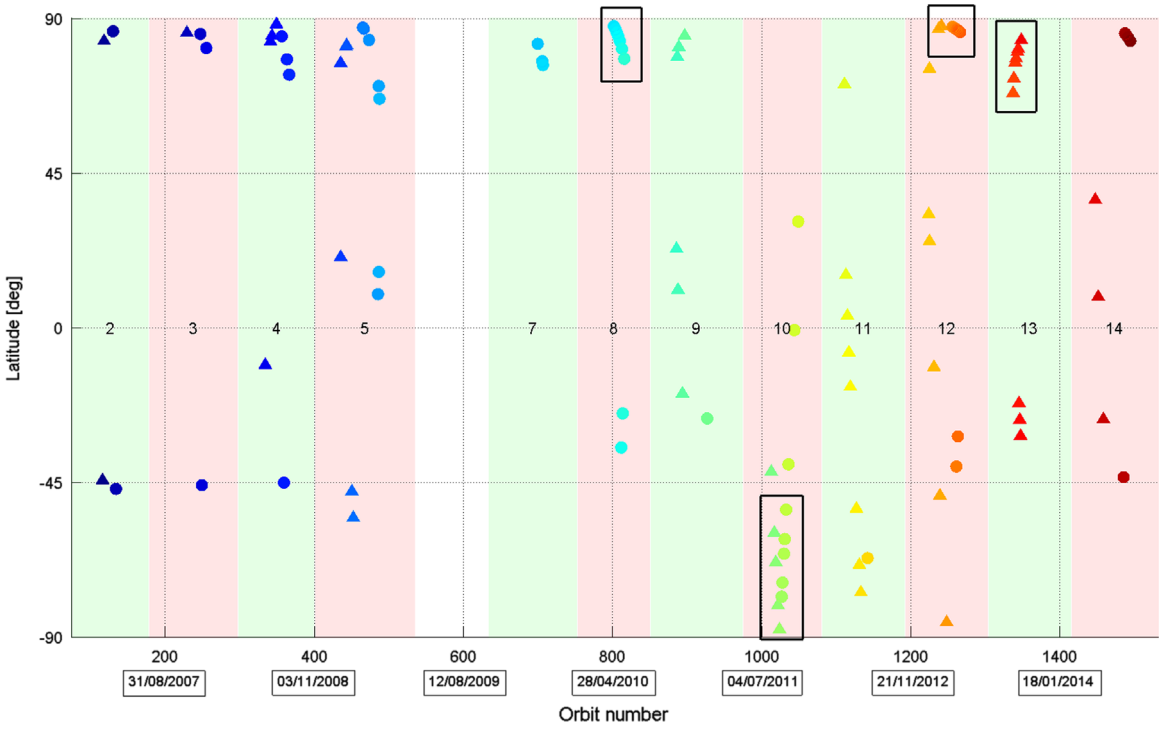

Fig. 9. CO observations performed during the first 14 occultation seasons. Orbit number and latitude of the observation are indicated. Each dot represents one occultation. The boxes indicate the observations selected for this study.

within the mesosphere via photochemical recombination to CO_2 through catalytic radical chemistry (Yung and DeMore, 1982), as illustrated by the evolution of the CO density and vmr in all figures. Two different regimes are observed for the CO evolution with altitude. The altitude of 95 km seems to be the transition, delimiting two regions where the slope of the CO density changes with altitude. Considering all observations, we have indeed obtained CO scale heights between 4 and 5 km below 95 km, and between 8 and 12 km above that altitude. The lower scale height obtained at lower altitudes is in very good agreement with the scale height obtained by Marcq et al. (2014) who found values of 3.5–4 km at an altitude of 70 km. The altitude of 95 km clearly delimits two regions where CO is behaving differently. This altitude also corresponds to the accepted transition between the strong zonal winds which dominate in the mesosphere of Venus and the SS-AS circulation driven by day-to-night temperature gradients.

The first striking feature seen is the high variability of the measured CO densities and vmrs, both within one group of observations, but also from OS to OS. For example higher day-to-day variability above 100 km is observed for the CO densities of OS 10 and OS 13 than those of OS 8. For some episodes, the CO densities vary considerably over relatively short periods of time: for example in OS 13, CO densities vary by more than a factor 10 at an altitude of 120 km, but since the same level of variability is also found, in this case, in the CO_2 density, the variability observed on the CO vmr is small. To illustrate the reality of the observed variability, spectra recorded during two nearly consecutive orbits

Table 1
Characteristics of the selected orbits: orbit number, date, ingress (IN) or egress (E), distances to Venus and to the limb, vertical resolution, latitude, local solar time (LST), orders recorded and indication of which species were targeted (a=CO_2, b=CO, c=HCl, d=HDO, e=H_2O, f=HF).

Orbit	Date	Type	Distance to Venus (km)	Distance to limb (km)	Vertical resolution (km)	Longitude (deg)	Latitude (deg)	LST (h)	Order 1	Order 2	Order 3	Order 4
OS8												
801	30/06/2008	E	632	2566	2	82	87.5	6	149a	130c	190b,f	114a
803	02/07/2008	E	636	2577	2	105	86.6	6	149a	130c	190b,f	115
805	04/07/2008	E	644	2597	2	120	85.4	6	149a	130c	190b,f	138
807	06/07/2008	E	656	2628	2	132	84.2	6	149a	130c	190b,f	139
809	08/07/2008	E	673	2671	2	143	82.8	6	149a	130c	190b,f	150
812	11/07/2008	E	712	2766	2	156	80.4	6	149a	130c	190b,f	177
815	14/07/2008	E	775	2919	2	169	77.3	6	149a	130c	190b,f	187b,f
OS10												
1012	27/01/2009	IN	9147	13889	8	245	−41.7	18	121d	149a	171e	190b,f
1016	31/01/2009	IN	10098	14924	9	256	−59.5	18	121d	149a	171e	190b,f
1018	02/02/2009	IN	10405	15256	9	261	−68.1	18	121d	149a	171e	190b,f
1026	10/02/2009	IN	10561	15424	9	121	−78.1	6	121d	149a	171e	190b,f
1027	11/02/2009	IN	10461	15316	9	122	−73.9	6	121d	149a	171e	190b,f
1029	13/02/2009	IN	10183	15016	9	125	−65.6	6	121d	149a	171e	190b,f
1030	14/02/2009	IN	10006	14824	9	127	−61.3	6	121d	149a	171e	190b,f
1032	16/02/2009	IN	9576	14357	8	132	−52.8	6	121d	149a	171e	190b,f
1035	19/02/2009	IN	8744	13447	8	140	−39.5	6	121d	149a	171e	190b,f
OS12												
1236	08/09/2009	E	248	1264	1	235	86.2	18	149a	130c	190b,f	152
1240	12/09/2009	E	237	1206	1	263	87.4	18	149a	130c	190b,f	152
1251	23/09/2009	E	220	1117	1	15	87.8	18	149a	109	110	111a
1255	27/09/2009	E	217	1101	1	44	87.2	6	149a	121d	171e	190b,f
1257	29/09/2009	E	216	1093	1	56	86.9	6	149a	121d	171e	190b,f
1259	01/10/2009	E	215	1087	1	67	86.5	6	149a	121d	171e	190b,f
1261	03/10/2009	E	214	1083	1	77	86.1	6	149a	121d	171e	190b,f
1263	05/10/2009	E	214	1081	1	87	85.7	6	149a	121d	171e	190b,f
1265	07/10/2009	E	214	1083	1	96	85.3	6	149a	121d	171e	190b,f
OS13												
1336	17/12/2009	IN	733	2817	2	165	68.9	18	148a	189b,f	190b,f	191b,f
1337	18/12/2009	IN	678	2682	2	168	70.9	18	148a	189b,f	190b,f	191b,f
1339	20/12/2009	IN	576	2415	2	173	74.6	18	148a	189b,f	190b,f	191b,f
1340	21/12/2009	IN	543	2325	2	175	76.0	18	148a	149a	150a	190b,f
1342	23/12/2009	IN	498	2193	2	180	78.3	18	148a	149a	150a	190b,f
1343	24/12/2009	IN	481	2143	1	182	79.3	18	148a	189b,f	190b,f	191b,f
1347	28/12/2009	IN	438	2006	1	189	82.4	18	148a	149a	150a	190b,f

(807 and 809) are shown in Fig. 14 for two altitudes. As can be seen, the absorption of CO is very different in these two orbits at similar altitudes. To better show the high variability of the observations, the standard deviations of the density and of the vmr of CO are plotted in Fig. 15. Plots were obtained for each OS separately (color curves) and for all data presented in this study (dark curve). As it can be seen the variability within one OS (short term variability) varies between 1.10 and 1.60 on the CO density and vmr for altitudes ranging from 100 to 115 km. The variability is expressed through the use of the geometric standard deviation, which has been chosen to describe how spread out are the values (density or vmr) for which the preferred average is obtained by calculating the geometric mean. In this case the geometric standard deviation is a dimensionless multiplicative number. The geometric standard deviation on the complete data set for those altitudes has a mean value of 1.5: observed density or vmr lie between the mean profile/1.5 and the mean profile × 1.5. Generally the variability of the CO density is higher and that of the CO vmr lower at higher altitudes. This is clearly seen for OS 12 (see Fig. 15). The variability of CO is not always reflected in that of CO_2.

In OS 12 and OS 13, the variation in time of the CO density is clearly visible (see Figs. 12 and 13, Panel A): in OS 12, the density increased from orbit 1240 to 1261 and started to decrease afterwards while in OS 13, the decrease of the density is taking place in a progressive way from orbit 1336 to 1347. However, the CO_2 density behaves quite significantly in different ways in these two OS: in OS 12 there is no clear evolution with time, whereas in OS 13, the CO_2 density follows the same trend as the CO density, decreasing smoothly with time. In that case, the resulting CO vmr varies much less.

As we showed in the previous section, the CO retrieval itself is not influenced by the temperature profile used during the analysis of the occultation spectra. The correlation observed between higher variability of CO abundance and of temperature is thus independent of the retrieval and appears to be real. For OS 8 there is a clear correlation between CO and CO_2 densities, as well as between CO and temperature, as shown in Fig. 16. The correlation between CO and CO_2 is clearly observed above 110 km (see Panel A), less below that altitude, whereas correlation between CO and temperature is present at all altitudes (see Panel B). The highest CO densities are associated to the highest temperatures at a given altitude. This would indicate that above 110 km the major process influencing CO is the photodissociation of CO_2, and that only below 110 km do other processes come into play. The correlation between CO_2 and temperature (see Panel C) is expected since the temperature has been retrieved from the CO_2 densities. The observed slopes is positive below 110 km and negative above that level, which can be explained by the temperature vertical profile (see Fig. 10, Panel D) showing a maximum at about 110 km altitude.

Clancy et al. (2012b) also reported high variability of temperature and CO mixing ratio, both spatially and temporally. They showed periods where up to 24 K and 133% spatial variations of the temperature and the CO vmr respectively were observed

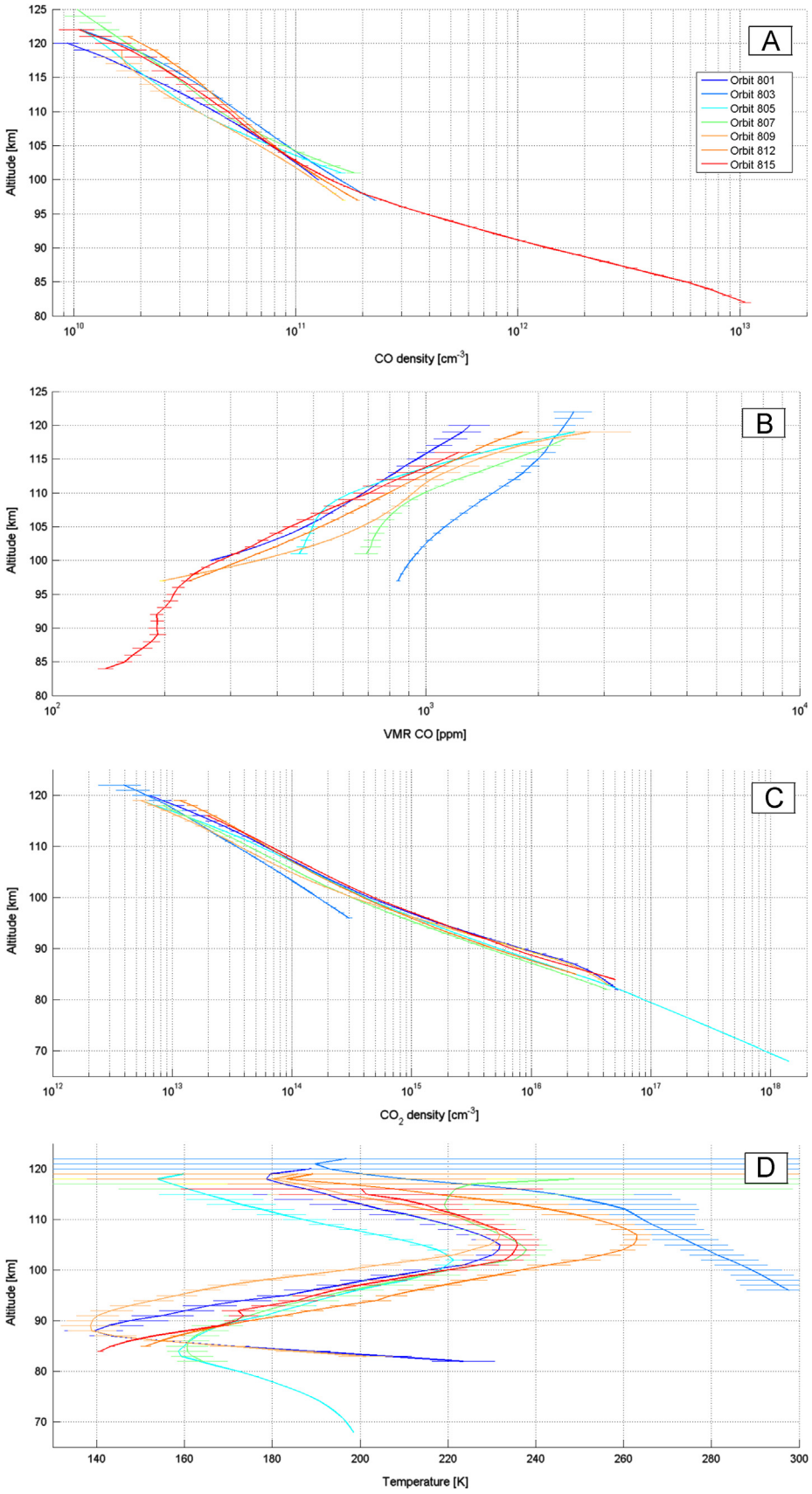

Fig. 10. CO densities (A) and vmr (B), CO_2 densities (C), and temperature (D) for the observations performed during OS 8 (orbits 801–815). The color indicates the orbit number. Depending on the choice of the orders (see Table 1) the profiles span different altitude ranges.

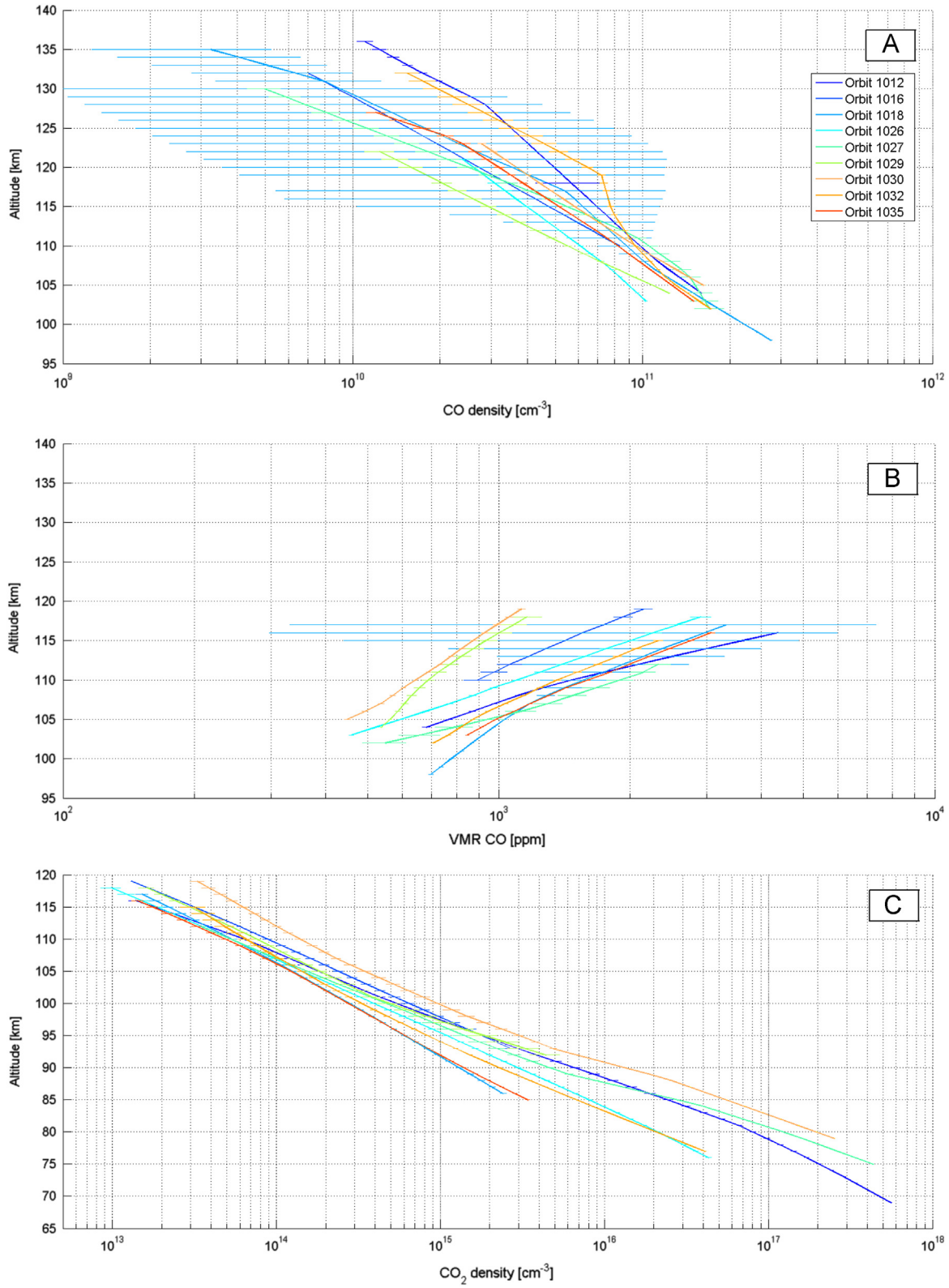

Fig. 11. CO densities (A) and vmr (B) as well as CO_2 densities (C) for the observations performed during OS 10 (orbits 1012–1035). The color indicates the orbit number. Depending on the choice of the orders (see Table 1) the profiles span different altitude ranges.

between 95 and 100 km. They also mentioned several cases of high temporal variability, with variations up to 100–200% (see for example Fig. 9D in Clancy et al. (2012b)). They definitively saw a correlation between a temperature increase above 95 km and a CO abundance increase. They associated this correlation to the strong downward vertical advection, drawing larger CO vmr at higher altitudes downward leading to a strong compressional adiabatic heating. In Tsang et al. (2009), CO abundances obtained from VIRTIS observations are reported at an altitude of ~35 km and show unexpected high variability in space and time. The accepted

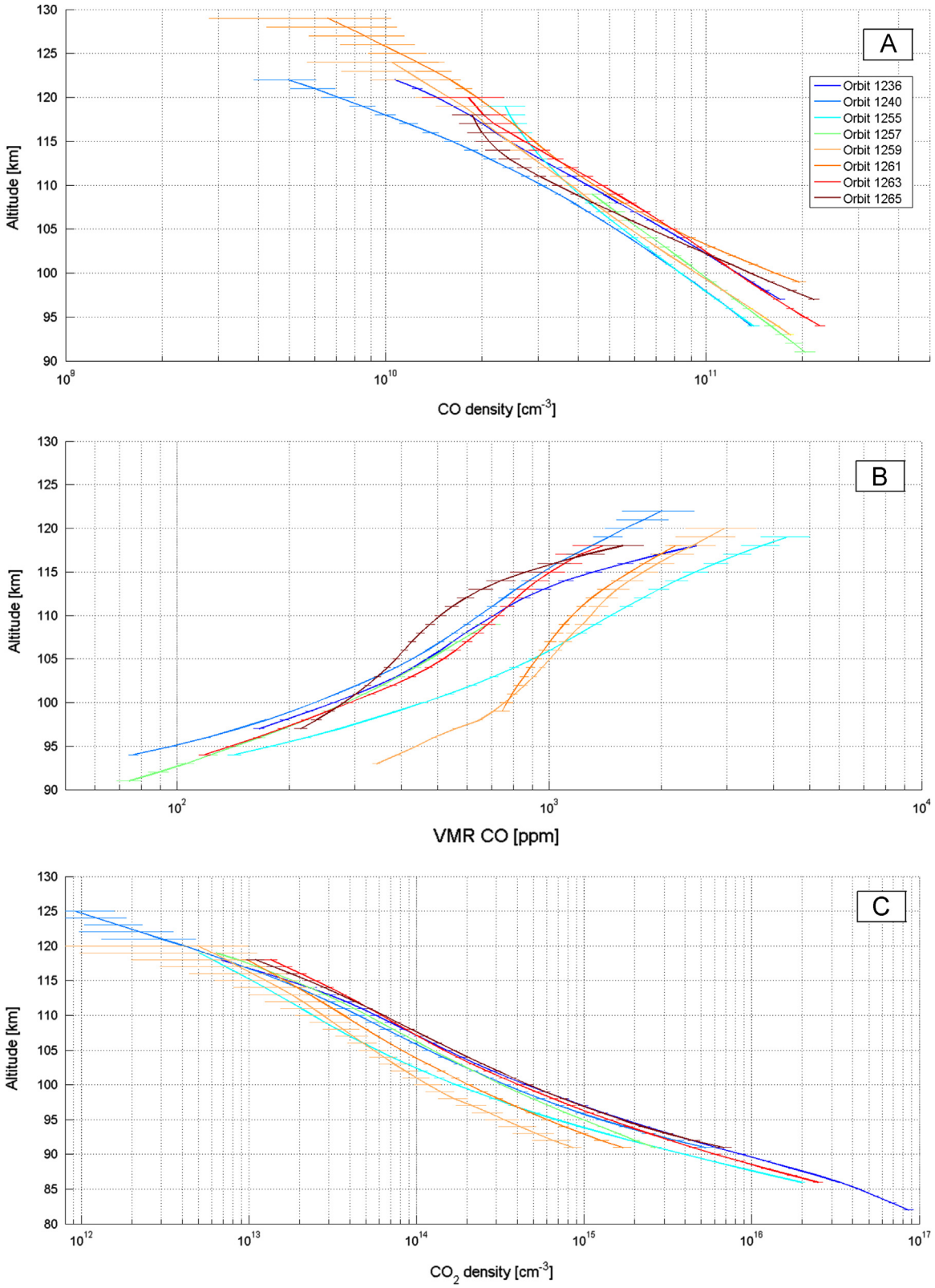

Fig. 12. CO densities (A) and vmr (B) as well as CO_2 densities (C) for the observations performed during OS 12 (orbits 1223–1265). The color indicates the orbit number. Depending on the choice of the orders (see Table 1) the profiles span different altitude ranges.

scenario was that a Hadley-type cell would bring enriched CO air from higher altitudes towards the lower layers of the atmosphere. However the variability seen at 35 km led the authors speculate that such a simple view was not consistent with the observations. They concluded that the meridional circulation could be more asymmetric than one single Hadley cell. This might imply that the strength of the downwelling might be variable. Such a complex circulation would also explain the high spatial and temporal

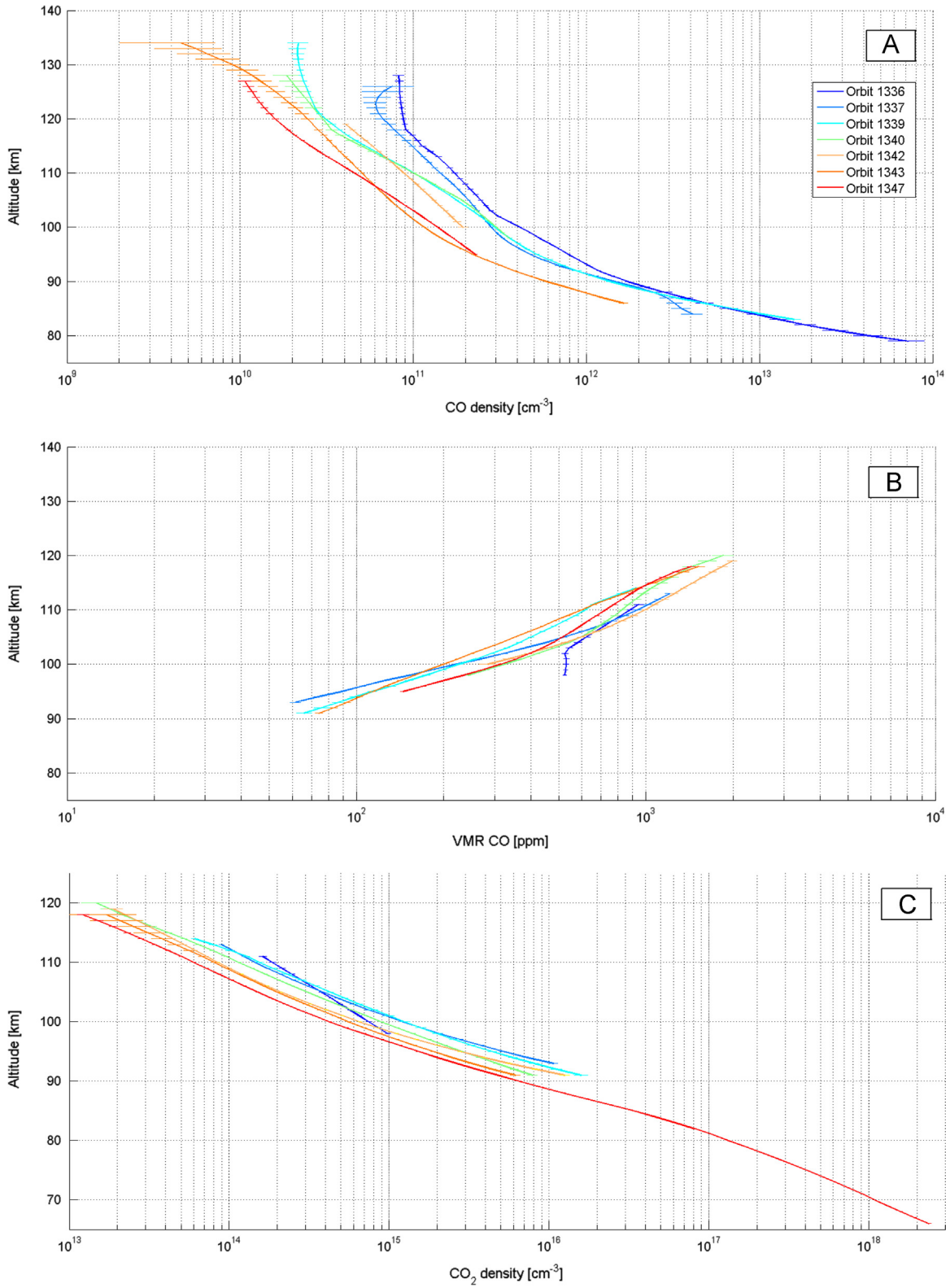

Fig. 13. CO densities (A) and vmr (B) as well as CO_2 densities (C) for the observations performed during OS 13 (orbits 1335–1347). The color indicates the orbit number. Depending on the choice of the orders (see Table 1) the profiles span different altitude ranges.

variability seen in the SOIR data. Another explanation could however lie in the existence of planetary waves.

The CO vmr and density profiles have also been compared with literature data. Results of this comparison are shown in Fig. 17. CO densities obtained by Gilli et al. (2015) from the analysis of the 4.7 μm non-LTE emission band of CO observed by VIRTIS-H are reproduced for the different local solar times (8 and 12 am, and 4 pm) and for the different latitude bins considered in Gilli et al.

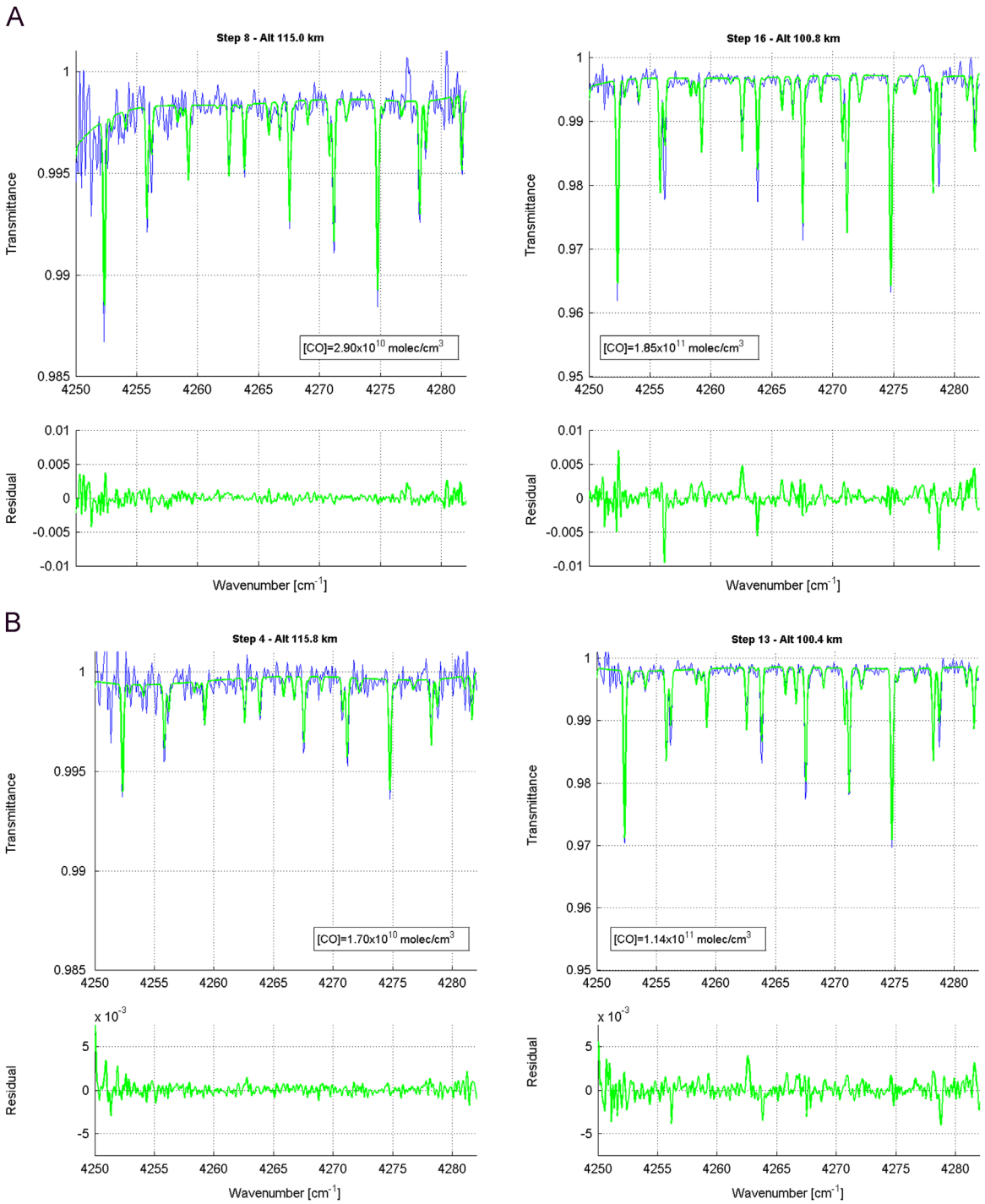

Fig. 14. Transmittances obtained for different altitudes during two nearly consecutive occultation 807 (top) and 809 (bottom): (a) around 100 km (right); (b) around 115 km (eft). In each case, the observed and fitted transmittances (blue and green respectively) are plotted in the upper panel and the residual in the bottom panel. Only the fitted CO absorption is considered, lines appearing in the residual are due to HF.

(2014). The best agreement with the SOIR data is found for the two curves corresponding to 8 am and 70–80N and 50–70N bins, which is comforting. The largest difference is observed with data corresponding to equatorial regions at 12 am, which would confirm the diurnal and latitudinal dependences previously observed by others. Krasnopolsky (2012)'s profile is in very good agreement from 65 km up to 110 km. Comparison with literature data concerning the CO vmr is also very conclusive. Irwin et al. (2008)'s value of 40 ± 10 ppm at 65–70 km and that of Krasnopolsky at 70 km (70 ppm) are compatible with the values observed by SOIR. A series of recent CO profiles obtained by the JCMT spectrometer have been provided (Clancy, private communication). These spectra have been obtained with the same instrument and in similar conditions, whilst not in the same year, as the data described and discussed in Clancy et al. (2012b). They all correspond to dayside observations with local time varying between 8 and 11.30 am. The vertical profile obtained by Marcq et al. (2005) from observations performed at the NASA Infrared Telescope Facility (IRTF) in Hawaii with the SpeX imaging spectrometer is also plotted in the figure. All these profiles confirm the high variability observed in the SOIR

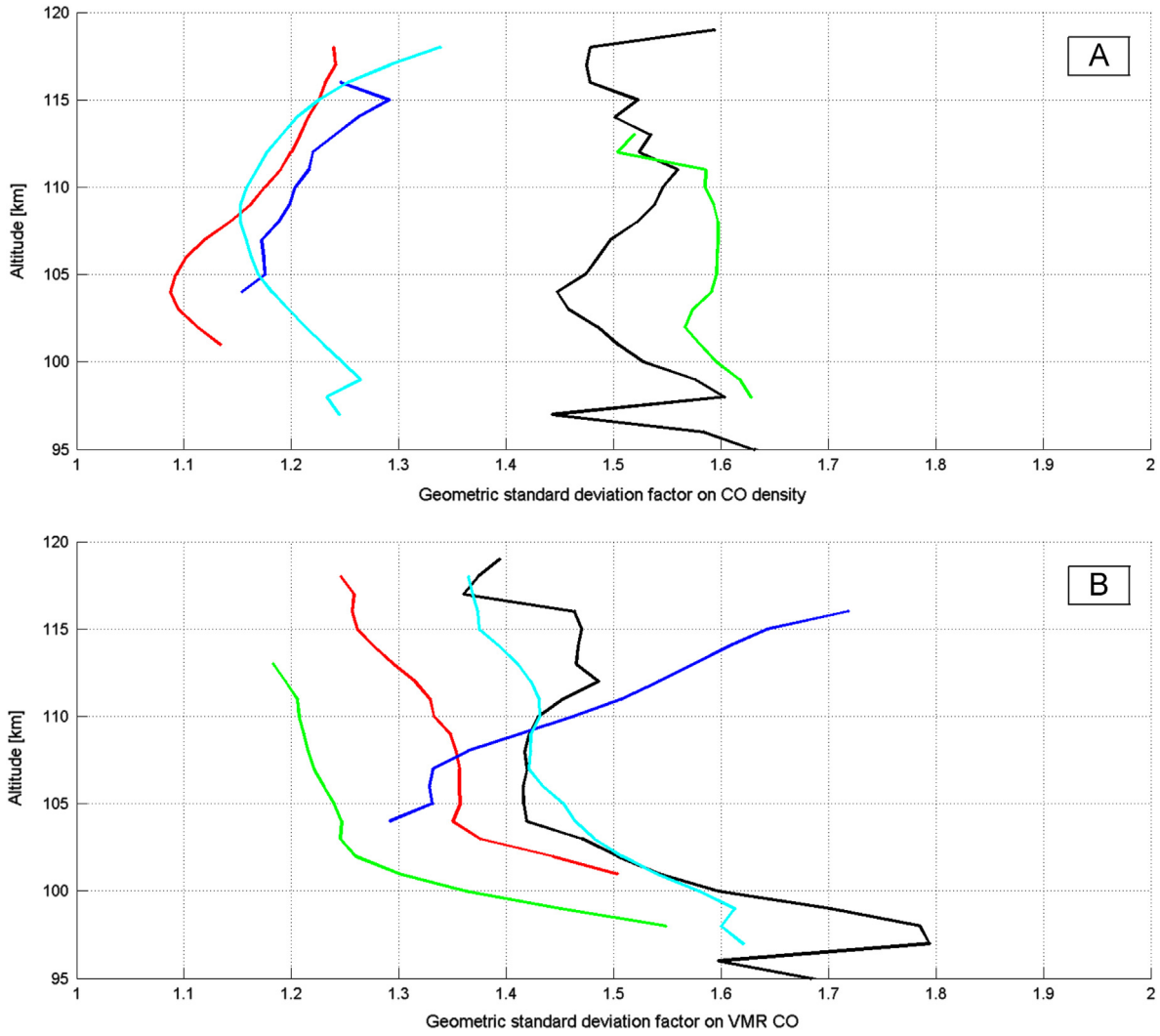

Fig. 15. Geometric standard deviation of the density (A) and of the vmr (B) of CO are shown as a function of altitude. Plots are shown for each OS (color curves: red – OS 08, blue – OS 10, cyan – OS 12, and green – OS 13) and for the complete data set (dark curve).

profiles and the occurrence of profiles of decreasing CO vmr down to lower altitudes.

6. Conclusions

CO densities and vmr have been measured by the SOIR instrument on board Venus Express on a regular basis since the beginning of the mission. Observations cover both hemispheres from 90S to 90N latitudes, but are all obtained at the terminator (LST 6 am and 6 pm). In this study we investigated the short term variability of CO by focussing on four periods of time where CO measurements were obtained close together. They correspond to high latitude observations. CO retrieval was described in detail and was shown to be independent of the temperature profiles used for the analysis of the spectra.

High variability from day to day but also from one occultation season to the other was demonstrated. Timescales involved are small, defined on a day-to-day basis. The region sounded by SOIR (65–150 km) corresponds to a region where different circulation patterns coexist: the SS-AS driven by strong diurnal temperature gradients, which is active essentially above 120 km, and the retrograde zonal circulation. The latter is active in the lower atmosphere (below 70 km). However it has been suggested that gravity waves, generated in the unstable cloud region, could force the retrograde zonal flow well above 70 km extending up to higher altitudes (Bougher et al., 2006). Lellouch et al. (1994) also suggested that a meridional component to the circulation might be present in the lower thermosphere. The circulation modeling of the Venus meso- and thermosphere is thus far from being fully understood. Clancy et al. (2012a, 2012b) performed CO, temperature and wind measurements in the lower thermosphere of Venus and reported that although the circulation in that region exhibits large-scale instability, there was no clear association between the amplitudes of the SS-AS and zonal winds and the observed temperature and CO spatial and temporal variability. They postulate the existence of a distinctive circulation pattern that would force large-scale air masses downward, creating dynamic increases in temperature and CO mixing ratio. This additional circulation would correlate with the timescale variations they observed on the nightside. Interestingly Hueso et al. (2008) showed that within O_2 airglow small-scale features ($\sim$100 km) were embedded in larger scale structures ($\sim$1000–3000 km) and seemed to be correlated to regions of strong subsidence associated with downward flows increasing the volume concentration of O atoms and inducing adiabatic warming, while the larger structures had their own motion characterized by timescale of a few hours with day-to-day changes. The transition region between the SS-AS and the retrograde zonal flow is thus far from being understood and will require additional efforts from modelers.

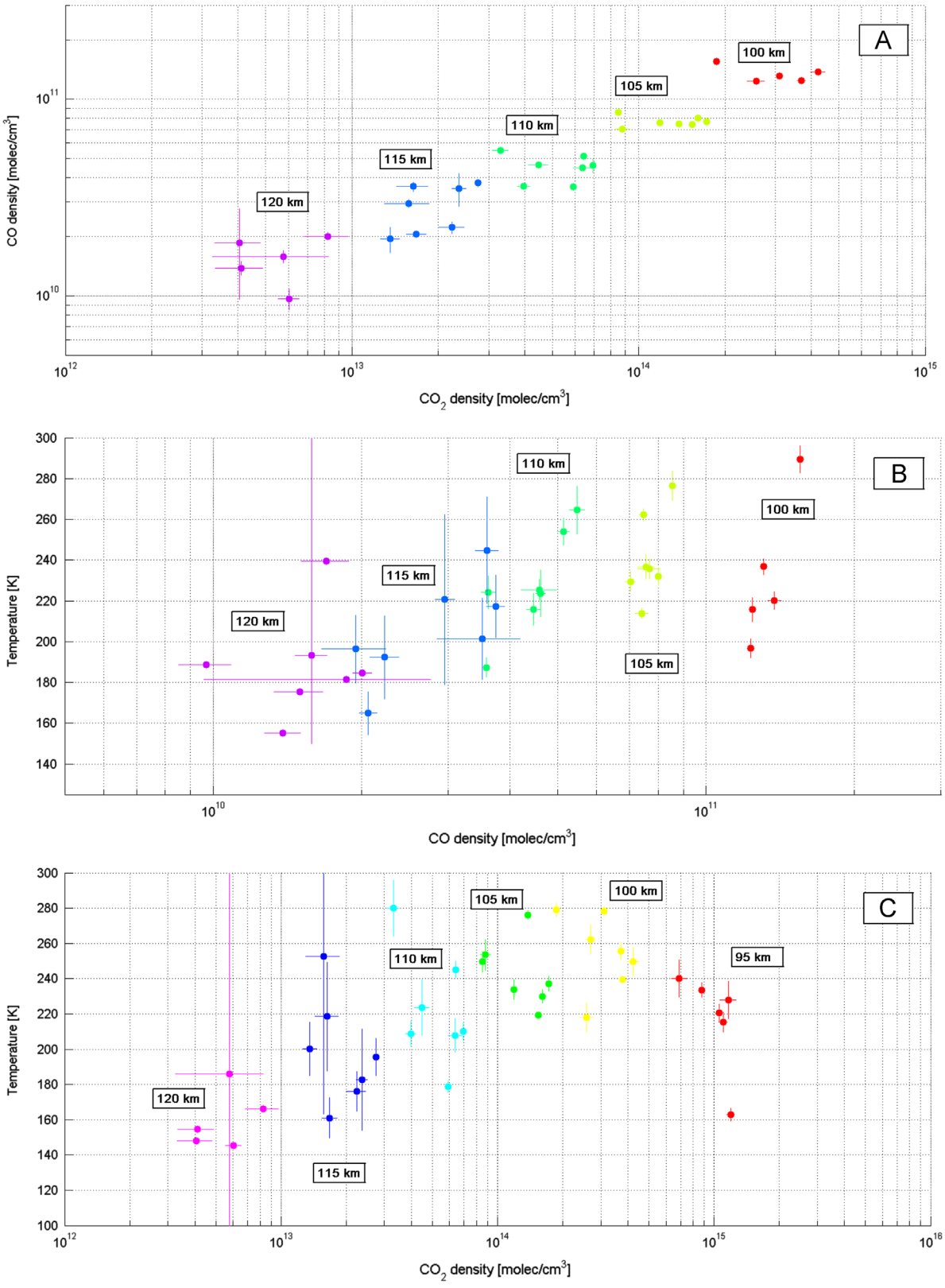

Fig. 16. Correlation between CO and CO_2 densities and temperature. The correlation between CO and CO_2 densities, temperature and CO densities, and temperature and CO_2 densities are plotted in Panels A, B, and C respectively, for different altitudes.

A clear correlation was found between CO abundance, CO_2 and temperature for altitudes above 110 km. The correlation is less pronounced for lower altitudes. This confirms that above 110 km the main process is the photodissociation of CO_2 to CO. This is also a confirmation that other processes in which CO is involved, such as cloud formation or participation in the catalytic cycles to recombine into CO_2, occur at lower altitudes. As an example Krasnopolsky (2012) indicates (Fig. 2 in Krasnopolsky (2012)) that CO_2 dissociation occurs at altitudes higher than 70 km and is the dominant process above 100 km, whereas the catalytic

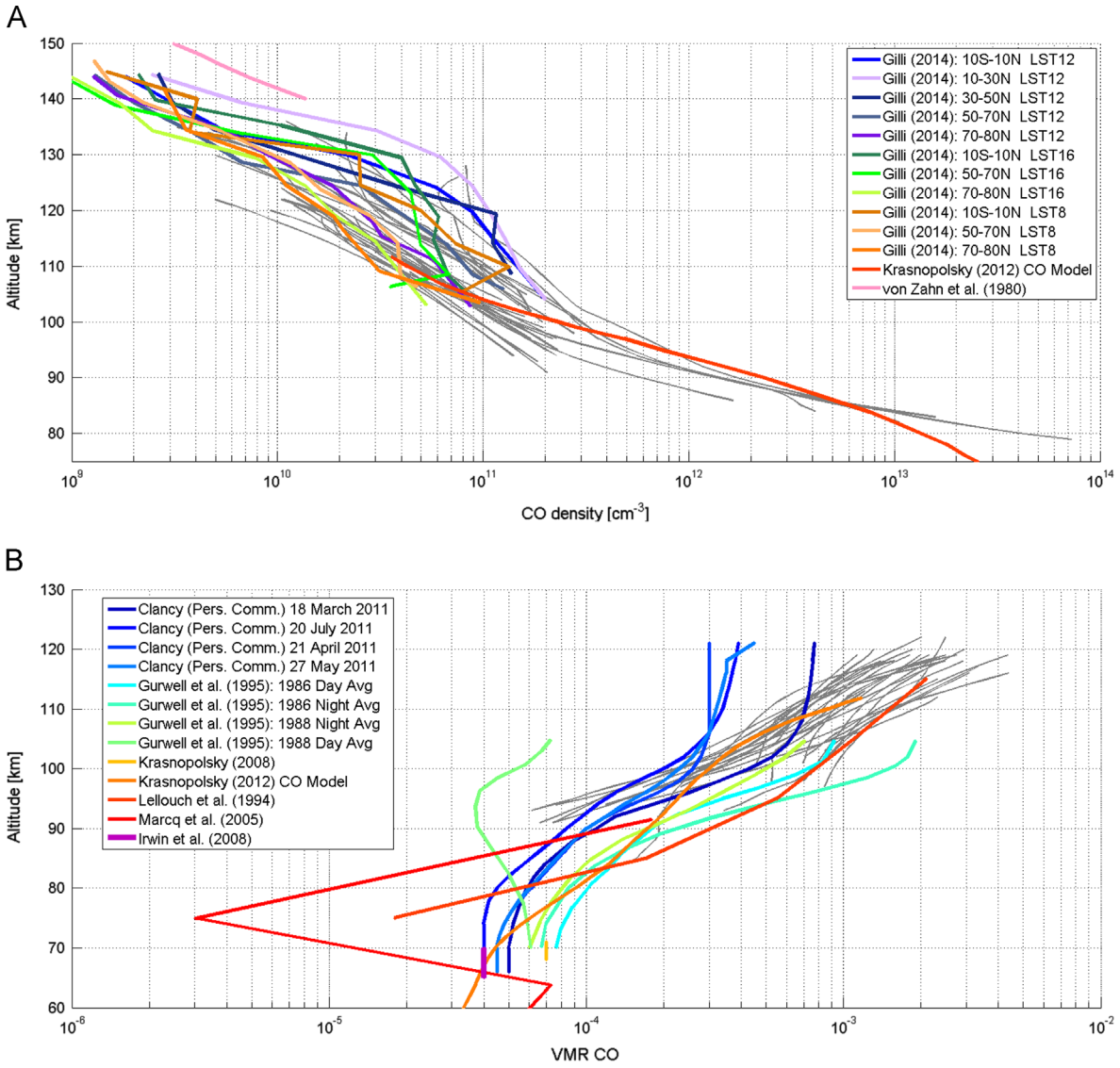

Fig. 17. Comparison with data from the literature: (top) density profiles obtained by Gilli et al. (submitted for publication) and the profile proposed by Krasnopolsky (2012); (bottom) several vmr vertical profiles from Clancy et al. (private communication) and previous observations (Connes et al., 1968; Gurwell et al., 1995; Irwin et al., 2008; Krasnopolsky, 2008; Lellouch et al., 1994; Marcq et al., 2005) and model (Krasnopolsky, 2012). All profiles from SOIR described in this study are plotted in gray.

recombination through ClCO is mostly active between 70 and 90 km, and the loss of CO in the cloud formation cycle has to be considered for even lower altitudes.

Observations performed by SOIR will hopefully help understand the processes and possible flow patterns, as they cover a very interesting region, i.e. the terminator separating the day and night sides on the planet. In near future this analysis will be extended to the complete CO data set obtained with SOIR. We will then be able to investigate the long term evolution of CO and the correlation existing between this species and others that have been measured either by SOIR or other instruments on board Venus Express.

Acknowledgments

The research program was supported by the Belgian Federal Science Policy Office and the European Space Agency (ESA – PRODEX Program – Contracts C 90323, 90113, and C4000107727). The research was performed as part of the "Inter-university Attraction Poles" program financed by the Belgian government (Planet TOPERS). The authors also recognize the support from the FP7 EuroVenus Project (G.A. 606798) as well as that of the HiResMIR International Scientific Coordination Network (GDRI).

References

Acton, C.H., 1996. Ancillary data services of NASA's navigational and ancillary information facility. Planet. Space Sci. 44, 65–70.

Bertaux, J.-L., Nevejans, D., Korablev, O., Villard, E., Quemerais, E., Neefs, E., Montmessin, F., Leblanc, F., Dubois, J.-P., Dimarellis, E., Hauchecorne, A., Lefevre, F., Rannou, P., Chaufray, J.Y., Cabane, M., Cernogora, G., Souchon, G., Semelin, F., Reberac, A., Van Ransbeeck, E., Berkenbosch, S., Clairquin, R., Muller, C., Forget, F., Hourdin, F., Talagrand, O., Rodin, A., Fedorova, A., Stepanov, A., Vinogradov, A. P., Kiselev, A., Kalinnikov, Y., Durry, G., Sandel, B.R., Stern, A., Gerard, J.-C., 2007a. SPICAV on Venus Express: three spectrometers to study the global structure and composition of the Venus atmosphere. Planet. Space Sci. 55, 1673–1700.

Bertaux, J.L., Nevejans, D., Korablev, O., Villard, E., Quémerais, E., Neefs, E., Montmessin, F., Leblanc, F., Dubois, J.P., Dimarellis, E., Hauchecorne, A., Lefevre, F., Rannou, P., Chaufray, J.Y., Cabane, M., Cernogora, G., Souchon, G., Semelina, F., Reberac, A., Van Ransbeek, E., Berkenbosch, S., Clairquin, R., Muller, C., Forget, F., Hourdin, F., Talagrand, O., Rodin, A., Fedorova, A., Stepanov, A., Vinogradov, A., Kiselev, A., Kalinnikov, Y., Durry, G., Sandel, B., Stern, A., Gérard, J.C., 2007b.

SPICAV on Venus Express: three spectrometers to study the global structure and composition of the Venus atmosphere. Planet. Space Sci. 55, 1673–1700.
Bézard, B., Baluteau, J.P., Marten, A., Coron, N., 1987. The $^{12}C/^{13}C$ and $^{16}O/^{18}O$ ratios in the atmosphere of Venus from high-resolution 10-mum spectroscopy. Icarus 72, 623–634.
Bézard, B., de Bergh, C., Crisp, D., Maillard, J.P., 1990. The deep atmosphere of Venus revealed by high-resolution nightside spectra. Nature 345, 508–511.
Bougher, S.W., Rafkin, S., Drossart, P., 2006. Dynamics of the Venus upper atmosphere: outstanding problems and new constraints expected from Venus Express. Planet. Space Sci. 54, 1371–1380.
Clancy, R.T., Muhleman, D.O., 1985. Diurnal CO variations in the Venus mesophere from CO microwave spectra. Icarus 64, 157–182.
Clancy, R.T., Muhleman, D.O., 1991. Long-term (1979–1990) changes in the thermal, dynamical and compositional structure of the Venus mesosphere as inferre from microwave spectral line observations of ^{12}CO, ^{13}CO, and $C^{18}O$. Icarus 89, 129–146.
Clancy, R.T., Sandor, B., Moriarty-Schieven, G., 2008. Venus upper atmospheric CO, temperature, and winds across the afternoon/evening terminator from June 2007 JCMT Sub-millimeter line observations. Planet. Space Sci. 56, 1344–1354.
Clancy, R.T., Sandor, B., Moriarty-Schieven, G., 2012a. Circulation of the Venus upper mesosphere/lower thermosphere: Doppler wind measurements from 2001 to 2009 inferior conjunction, sub-millimeter CO absorption line observations. Icarus 217, 794–812.
Clancy, R.T., Sandor, B., Moriarty-Schieven, G., 2012b. Thermal structure and CO distribution for the Venus mesosphere/lower thermosphere: 2001–2009 inferior conjunction sub-millimeter CO absorption line observations. Icarus 217, 779–793.
Connes, P., Connes, J., Kaplan, L., Benedict, W.S., 1968. Carbon monoxide in the Venus atmosphere. Astrophys. J. 152, 731–743.
Crovisier, J., Lellouch, E., de Bergh, C., Maillard, J.-P., Lutz, B.L., Bézard, B., 2006. Carbon monoxide emissions at 4.7 μm from Venus' atmosphere Planet. Space Sci. 54, 1398–1414.
Fedorova, A., Korablev, O., Vandaele, A.C., Bertaux, J.L., Belyaev, D., Mahieux, A., Neefs, E., Wilquet, V., Drummond, R., Montmessin, F., Villard, E., 2008. HDO and H_2O vertical distributions and isotopic ratio in the Venus mesosphere by solar occultation at infrared spectrometer onboard Venus Express. J. Geophys. Res. 113, http://dx.doi.org/10.1029/2008JE003146.
Gilli, G., 2012. Carbon Monoxide and Temperature in the Upper Atmosphere of Venus through the Analysis of Limb Observations by VIRTIS/Venus Express. Instituto de Astrof´ısica de Andaluc´ia, Universidad de Granada, Granada.
Gilli, G., Lopez-Valverde, M.A., Peralta, J., Bougher, S.W., Brecht, A., Drossart, P., Piccioni, G., 2015. Carbon monoxide and temperature in the upper atmosphere of Venus from VIRTIS/Venus Express non-LTE limb measurements. Icarus 248, 478–498.
Gurwell, M., Muhleman, D.O., Shah, K., Berge, G., Rudy, D.J., Grossman, A.W., 1995. Observations of the CO bulge on Venus and implications for mesospheric winds. Icarus 115, 141–158.
Hase, F., Wallace, L., McLeod, S., Harrison, J.J., Bernath, P., 2010. The ACE-FTS atlas of the infrared solar spectrum. J. Quant. Spectrosc. Radiat. Transf. 111, 521–528.
Hedin, A.E., Niemann, H.B., Kasprzak, W.T., 1983. Global empirical model of the Venus thermosphere. J. Geophys. Res. 88, 73–83.
Hueso, R., Sanchez-Lavega, A., Piccioni, G., Drossart, P., Gérard, J.-C., Khatuntsev, I., Zasova, L.V., Migliorini, A., 2008. Morphology and dynamics of Venus oxygen airglow from Venus Express/Visible and Infrared Thermal Imaging Spectrometer observations. J. Geophys. Res. 113, http://dx.doi.org/10.1029/2008JE003081.
IASB-BIRA, 2013. ASIMUT-ALVL Documentation.
Irwin, P.G.J., de Kok, K., Negrao, A., Tsnag, C., Wilson, C.F., Drossart, P., Piccioni, G., Grassi, D., Taylor, F.W., 2008. Spatial variability of carbon monoxide in Venus' mesosphere from Venus Express/VIRTIS measurements. J. Geophys. Res. 113, http://dx.doi.org/10.1029/2008JE003093.
Iwagami, N., Yamaji, T., Ohtsuki, S., Hashimoto, G.L., 2010. Hemispherical distribution of CO above the Venus' clouds by ground-based 2.3 μm spectroscopy. Icarus 207, 558–563.
Krasnopolsky, V., Parshev, V.A., 1983. Photochemistry of the Venus atmosphere. In: Hunten, D.M., Colin, L., Donahue, T.M., Moroz, L.V. (Eds.), Venus. University of Arizona Press, Tucson, pp. 431–458.
Krasnopolsky, V.A., 2008. High-resolution spectroscopy of Venus: detection of OCS, upper limit to H_2S, and latitudinal variations of CO and HF in the upper cloud layer. Icarus 197, 377–385.
Krasnopolsky, V.A., 2012. A photochemical model for the Venus atmosphere at 47–112 km. Icarus 218, 230–246.
Lellouch, E., Goldstein, J., Rosenqvist, J., Bougher, S.W., Paubert, G., 1994. Global circulation, thermal structure and carbon monoxide distribution in Venus' mesosphere in 1991. Icarus 110, 315–339.
Mahieux, A., 2011. Inversion of the Infrared Spectra Recorded by the SOIR Instrument on Board Venus Express (thesis). Univ. Libre de Bruxelles, Belgium.
Mahieux, A., Berkenbosch, S., Clairquin, R., Fussen, D., Mateshvili, N., Neefs, E., Nevejans, D., Ristic, B., Vandaele, A.C., Wilquet, V., Belayev, D., Fedorova, A., Korablev, J.-L., Villard, E., Montmessin, F., Bertaux, J.-L., 2008. In-flight performance and calibration of SPICAV SOIR on board Venus Express. Appl. Opt. 47, 2252–2265.
Mahieux, A., Vandaele, A.C., Bougher, S.W., Drummond, R., Robert, S., Wilquet, V., Piccialli, A., Montmessin, F., Tellmann, S., Pätzold, M., Häusler, B., Bertaux, J.L., 2015. Update of the Venus density and temperature profiles at high altitude measured by SOIR on board Venus Express. Planet. Space Sci. 113–114, 310–321.
Mahieux, A., Vandaele, A.C., Drummond, R., Robert, S., Wilquet, V., Fedorova, A., Bertaux, J.L., 2010. Densities and temperatures in the Venus mesosphere and lower thermosphere retrieved from SOIR onboard Venus Express: retrieval technique. J. Geophys. Res. 115, http://dx.doi.org/10.1029/2010JE003589.
Mahieux, A., Vandaele, A.C., Robert, S., Wilquet, V., Drummond, R., Montmessin, F., Bertaux, J.L., 2012. Densities and temperatures in the Venus mesosphere and lower thermosphere retrieved from SOIR on board Venus Express: carbon dioxide measurements at the Venus terminator. J. Geophys. Res. 117, http://dx.doi.org/10.1029/2012JE004058.
Marcq, E., Bertaux, J.L., Belyaev, D., Montmessin, F., Lellouch, E., Encrenaz, T., 2014. Compositional variability of the Venusian atmosphere above the clouds: sulphur dioxide and carbon monoxide. In: Proceedings of the 40th COSPAR. Moscou, Russia, 2–10 August.
Marcq, E., Bézard, B., Encrenaz, T., Birlan, M., 2005. Latitudinal variations of CO and OCS in the lower atmosphere of Venus from near-infrared nightside spectroimaging. Icarus 179, 375–386.
Marcq, E., Encrenaz, T., Bézard, B., Birlan, M., 2006. Remote sensing of Venus' lower atmosphere from ground-based IR spectroscopy: latitudinal and vertical distribution of minor species. Planet. Space Sci. 54, 1360–1370.
Mills, F.P., Allen, M., 2007. A review of selected issues concerning the chemistry in Venus' middle atmosphere. Planet. Space Sci. 55, 1729–1740.
Mills, F.P., Esposito, L.W., Yung, Y.L., 2007. Atmospheric composition, chemistry and clouds. Geophys. Monogr. Ser. 176, 73–100.
Nevejans, D., Neefs, E., Van Ransbeeck, E., Berkenbosch, S., Clairquin, R., De Vos, L., Moelans, W., Glorieux, S., Baeke, A., Korablev, O., Vinogradov, I., Kalinnikov, Y., Bach, B., Dubois, J.P., Villard, E., 2006. Compact high-resolution space-borne echelle grating spectrometer with AOTF based on order sorting for the infrared domain from 2.2 to 4.3 μm. Appl. Opt. 45, 5191–5206.
Pollack, J.B., Dalton, J.B., Grinspoon, D.H., Wattson, R.B., Freedman, R., Crisp, D., Allen, D.A., Bézard, B., de Bergh, C., Giver, L.P., Ma, Q., Tipping, R., 1993. Near-infrared light from Venus' nightside: a spectroscopic analysis. Icarus 103, 1–42.
Rodgers, C.D., 1990. Characterization and error analysis of profiles retrieved from remote sounding measurements. J. Geophys. Res. 95, 5587–5595.
Rodgers, C.D., 2000. Inverse Methods for Atmospheric Sounding: Theory and Practice. University of Oxford.
Rothman, L.S., Gordon, I.E., Barbe, A., Benner, D.C., Bernath, P.F., Birk, M., Boudon, V., Brown, L.R., Campargue, A., Champion, J.P., Chance, K.V., Coudert, L.H., Dana, V., Devi, V.M., Fally, S., Flaud, J.-M., Gamache, R., Goldman, A., Jacquemart, D., Kleiner, I., Lacome, N., Lafferty, W., Mandin, J.-Y., Massie, S., Mikhailenko, S., Miller, C., Moazzen-Ahmadi, N., Naumenko, O., Nikitin, A., Orphal, J., Perevalov, V., Perrin, A., Predoi-Cross, A., Rinsland, C.P., Rotger, M., Simeckova, M., Smith, M.A.H., Sung, K., Tashkun, S., Tennyson, J., Toth, R.A., Vandaele, A.C., Vander Auwera, J., 2009. The HITRAN 2008 molecular spectroscopic database. J. Quant. Spectrosc. Radiat. Transf. 110, 533–572.
Seiff, A., Schofield, J.T., Kliore, A., Taylor, F.W., Limaye, S.S., Revercomb, H.E., Sromovsky, L.A., Kerzhanovich, V.V., Moroz, V.I., Marov, M.Y., 1985. Models of the structure of the atmosphere of Venus from the surface to 100 km altitude. Adv. Space Res. 5, 3–58.
Sung, K., Varanasi, P., 2005. CO_2-broadened half-widths and CO_2-induced line shifts of $^{12}C^{16}O$ relevant to the atmospheric spectra of Venus and Mars. J. Quant. Spectrosc. Radiat. Transf. 91, 319–322.
Titov, D.V., et al., 2006. Venus Express science planning. Planet. Space Sci. 54, 1279–1297.
Tsang, C.C.C., Taylor, F.W., Wilson, C.F., Liddell, S.J., Irwin, P.G.J., Piccioni, G., Drossart, P., Calcutt, S., 2009. Variability of CO concentrations in the Venus troposphere from Venus Express/VIRTIS using a band ratio technique. Icarus 201, 432–443.
Vandaele, A.C., De Mazière, M., Drummond, R., Mahieux, A., Neefs, E., Wilquet, V., Korablev, O., Fedorova, A., Belyaev, D., Montmessin, F., Bertaux, J.L., 2008. Composition of the Venus mesosphere measured by SOIR on board Venus Express. J. Geophys. Res. 113, http://dx.doi.org/10.1029/2008JE003140.
Vandaele, A.C., Mahieux, A., Robert, S., Berkenbosch, S., Clairquin, R., Drummond, R., Letocart, V., Neefs, E., Ristic, B., Wilquet, V., Colomer, F., Belyaev, D., Bertaux, J.L., 2013. Improved calibration of SOIR/Venus Express spectra. Opt. Express 21, 21148.
Wilquet, V., Drummond, R., Mahieux, A., Robert, S., Vandaele, A.C., Bertaux, J.L., 2012. Optical extinction due to aerosols in the upper haze of Venus: four years of SOIR/VEX observations from 2006 to 2010. Icarus 217, 875–881.
Wilquet, V., Fedorova, A., Montmessin, F., Drummond, R., Mahieux, A., Vandaele, A. C., Villard, E., Korablev, O., Bertaux, J.L., 2009. Preliminary characterization of the upper haze by SPICAV/SOIR solar occultation in UV to mid-IR onboard Venus Express. J. Geophys. Res. 114, http://dx.doi.org/10.1029/2008JE003186.
Yung, Y.L., DeMore, W.B., 1982. Photochemistry of the stratosphere of Venus: implications for atmospheric evolution. Icarus 51, 199–247.